

AD-A128-435

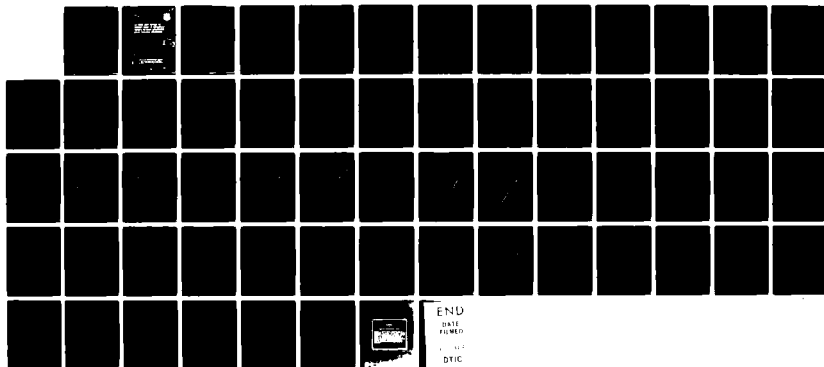
SCATTERING CROSS SECTIONS FOR COMPOSITE MODELS OF
NON-GAUSSIAN SURFACES F. (U) NEBRASKA UNIV LINCOLN
E BAHAR ET AL. MAR 83 RADC-TR-83-47 F19628-81-K-0025

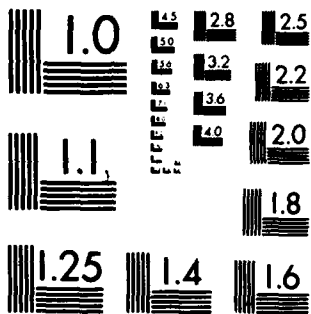
1/1

UNCLASSIFIED

F/G 20/14

NL





MICROCOPY RESOLUTION TEST CHART
NATIONAL BUREAU OF STANDARDS-1963-A

AD A128485

SCATTERING CROSS SECTION FOR
COMPOSITE MODELS OF NON-UNIFORM
SURFACES FOR WHICH DECORRELATION
IMPLIES STATISTICAL INDEPENDENCE

SCATTERING CROSS SECTION FOR COMPOSITE MODELS OF NON-UNIFORM SURFACES FOR WHICH DECORRELATION IMPLIES STATISTICAL INDEPENDENCE

University of Nebraska-Lincoln

Richard Baker
Mary Ann Plummer

APPROX 100 PAGES

PHOTOCOPY



This report has been reviewed by the RADC Office and is approved for release to the National Technical Information Administration. It will be available to the general public.

RADC-TR-33-47 has been revised and is approved for publication.

APPROVED: *K.V.N. Rao*
K.V.N. RAO
Project Engineer

APPROVED: *Allan C. Schell*
ALLAN C. SCHELL
Chief, Electromagnetic Sciences Division

FOR THE COMMANDER: *John P. Huss*
JOHN P. HUSS
Acting Chief, Plans Office

If your address has changed or if you wish to be removed from the RADC mailing list, or if the address is no longer correct for your organization, please notify RADC (HRT) Room 404 NE 17th. This will assist us in maintaining a current mailing list.

Do not remove copies of this report unless contractual obligations or other specific document criteria that is to be retained.

UNCLASSIFIED

SECURITY CLASSIFICATION OF THIS PAGE(When Data Entered)

polarized cross sections have the same dependence on the special form of the surface height joint probability density, but for large angles the scattering cross sections for the horizontally polarized waves are much more sensitive to the special form of the joint probability density. The corresponding results for the depolarized backscatter cross section are also presented. The shadow functions are shown to be rather insensitive to the special form of the joint probability density.

ERIC
COPY
AVAILABLE

Accession For	
NTIS GRA&I	
DTIC TAB	
Unannounced	
Justification	
By	
Distribution/	
Availability Codes	
Dist	Avail and/or Special
A	

UNCLASSIFIED

SECURITY CLASSIFICATION OF THIS PAGE(When Data Entered)

1. Introduction

In this work the full wave approach is used to determine the scattering cross sections for composite models of non-Gaussian rough surfaces. In particular, it is assumed here that the rough surface is characterized by a family of joint height probability densities that have been developed by Beckmann (1973a,b) for non-Gaussian surfaces. These joint height probability densities are expressed as an infinite sum of powers of the correlation coefficient and it is assumed that decorrelation of surface heights implies statistical independence. Using these joint probability density functions, Beckmann (1973a,b) derives physical optics and geometrical optics approximations for the scattering cross sections. Recently, Brown considered rough surfaces with exponential joint height probability densities (Brown, 1982). In his work Brown concludes that the appearance of a delta function type specular term in his results "suggests that decorrelation does indeed imply statistical independence for real surfaces."

In Section 2 the principal elements of the full wave approach are summarized. In Sections 3 and 4, the expressions for the marginal slope densities and the shadow functions for the non-Gaussian surfaces are derived. In Section 5 illustrative examples are presented. By considering a very broad family of non-Gaussian rough surfaces that include in the limits the exponential and the Gaussian surfaces, it is possible to derive the full wave solutions for the backscatter cross sections for more realistic models of rough surfaces. Since it is assumed in this work that decorrelation of the surface heights implies statistical

independence, no delta function type specular terms are obtained in these results. It is found that for angles of incidence $\theta_o^1 > 25^\circ$, the backscatter cross section for the horizontally polarized waves are more sensitive to the specific form of the joint height probability density assumed. The reason for this is given in Section 5. For near normal incidence both the backscatter cross sections for vertically and horizontally polarized waves, exhibit the same dependence on the special form of the joint height probability density assumed. The depolarized backscatter cross sections are sensitive to the special form of the surface statistics only near normal incidence.

It is interesting to note that for the mean square slopes considered in the illustrative examples, the shadow functions for the non-Gaussian surfaces are practically indistinguishable from the shadow function for the Gaussian surface, nevertheless the backscatter cross sections are sensitive to the precise form of the surface height statistics assumed (see Section 5).

2. Formulation of the Problem

The full wave solutions for the scattering cross sections are summarized in this section for a two scale model of random rough surfaces $h(x,z)$ (See Fig. 1) (Bahar et al 1982). To this end consider the Fourier transform of the surface height autocorrelation function $\langle h(x,z)h'(x',z') \rangle$ which is the surface height spectral density function (Rice 1951)

$$W(v_x, v_z) = \frac{1}{\pi^2} \int_{-\infty}^{\infty} \exp(iv_x x_d + iv_z z_d) \langle h(x,z)h'(x',z') \rangle dx_d dz_d \quad (2.1)$$

In (2.1) the symbol $\langle \rangle$ denotes statistical average and

$$\bar{v} = k_0 (\bar{n}^f - \bar{n}^i) = v_x \bar{a}_x + v_y \bar{a}_y + v_z \bar{a}_z, \quad |\bar{v}| = v \quad (2.2a)$$

in which \bar{n}^i and \bar{n}^f are unit vectors in the directions of the incident and scattered waves

$$\bar{n}^i = \sin\theta_0^i \cos\phi^i \bar{a}_x - \cos\theta_0^i \bar{a}_y + \sin\theta_0^i \sin\phi^i \bar{a}_z = \bar{k}^i/k_0 \quad (2.2b)$$

$$\bar{n}^f = \sin\theta_0^f \cos\phi^f \bar{a}_x + \cos\theta_0^f \bar{a}_y + \sin\theta_0^f \sin\phi^f \bar{a}_z = \bar{k}^f/k_0 \quad (2.2c)$$

and $k_0 = \omega(\epsilon_0 \mu_0)^{1/2}$ is the free space wavenumber characterized by the permittivity ϵ_0 and permeability μ_0 . An $\exp(i\omega t)$ time dependence is assumed in this work.

The distance between two points in the reference (x,z) plane is

$$r_d = |\bar{r}_d| = |x_d \bar{a}_x + z_d \bar{a}_z| = |(x-x')\bar{a}_x + (z-z')\bar{a}_z| \quad (2.3)$$

For convenience the rough surface height $h(x,z)$ is decomposed into two parts

$$h(x,z) = h_\ell(x,z) + h_s(x,z) \quad (2.4)$$

the first term h_ℓ consists of the large scale spectral components

$$0 \leq k^2 \equiv v_x^2 + v_z^2 \leq k_d^2 \quad (2.5)$$

where k_d is the wavenumber where spectral splitting is assumed to occur (Brown 1978, 1980). In this work the wavenumber k_d is chosen such that

the surface h_ρ meets the radii of curvature criteria (associated with the Kirchhoff approximations for the surface fields). It is also assumed here that the surface h_ρ meets the condition for deep phase modulation (Bahar et al 1982). The second term in (2.4), h_g , consists of the small scale spectral components

$$k_d < k \leq k_c \quad (2.6)$$

where k_c is the spectral cutoff wavenumber (Brown 1978). The full wave scattering cross section for the composite surface (2.4) which accounts for both specular scatter and Bragg scatter in a self-consistent manner is given by the weighted sum of two cross sections (Bahar et al 1982)

$$\langle \sigma^{PQ} \rangle_T = \langle \sigma^{PQ} \rangle_O + \langle \sigma^{PQ} \rangle_R \quad (2.7)$$

in which the first and second superscripts (P and Q, V for vertical, H for horizontal) denote the polarization of the scattered and incident waves respectively. The first term in (2.7) is the scattering cross section associated with the surface h_ρ . Thus

$$\langle \sigma^{PQ} \rangle_O = |\chi^s(v)|^2 \langle \sigma_\infty^{PQ} \rangle \quad (2.8)$$

where

$$\langle \sigma_\infty^{PQ} \rangle = \frac{4\pi k_o^2}{v_y^2} \left[\left| \frac{D^{PQ}}{\bar{n} \cdot \bar{a}_y} \right|^2 P_2(\bar{n}^f, \bar{n}^i | \bar{n}) P(\bar{n}) \right]_{\bar{n} \rightarrow \bar{n}_s} \quad (2.9)$$

In (2.8) the characteristic function for the surface h_g , $\chi^s(v)$, has the effect of decreasing the contribution of the physical optics scattering cross section $\langle \sigma_\infty^{PQ} \rangle$. As $\langle h_g^2 \rangle$, the mean square of the small scale surface height (that rides on the large scale surface h_ρ), approaches zero, $|\chi^s|^2 \rightarrow 1$. It is assumed in this work that the small scale surface height, h_g , has a Gaussian distribution and in this case the coefficient $|\chi^s|^2$ in (2.8) is

$$|\chi^s(v)|^2 = |\langle \exp iv h_s \rangle|^2 = \exp(-4k_0^2 \langle h_s^2 \rangle) = \exp(-\beta) \quad (2.10)$$

Thus the effective weighting function, $|\chi^s|^2$, decreases monotonically as $\beta = 4k_0^2 \langle h_s^2 \rangle$ increases. The shadow function $P_2(\bar{n}^f, \bar{n}^i | \bar{n})$ is the probability that a point on the rough surface is both illuminated by the source and visible at the observation point given the value of the slopes h_x, h_z at that point (Smith 1967, Sancer 1969). The unit vector normal to the rough surface is

$$\begin{aligned} \bar{n} &= \nabla(y-h_\ell(x,z)) / |\nabla(y-h_\ell(x,z))| \approx \nabla(y-h(x,z)) / |\nabla(y-h(x,z))| \\ &= (-h_x \bar{a}_x + \bar{a}_y - h_z \bar{a}_z) / (h_x^2 + 1 + h_z^2)^{1/2} \end{aligned} \quad (2.11a)$$

where

$$h_x = \partial h / \partial x, \quad h_z = \partial h / \partial z \quad (2.11b)$$

and

$$\bar{n}_s = \bar{v} / v \quad (2.11c)$$

is the value of \bar{n} at the specular points of the rough surface. Furthermore, $p(\bar{n}) = p(h_x, h_z)$ is the joint probability density function for the slopes of the large scale surface h_ℓ . In this work the joint probability density function for the large scale surface height $h_\ell(x,z)$ and its associated slope distribution function are assumed to be either Gaussian or non-Gaussian (Beckmann 1973a,b, see Section 3).

The coefficient D^{PQ} in (2.9) depends on the polarization of the scattered and incident waves, the unit vectors \bar{n}^i, \bar{n}^f and \bar{n} and the permittivity ϵ and permeability μ of the media above and below the rough surface $h(x,z)$ (Bahar 1981a,b).

The second term in (2.7) is the scattering cross section associated with the small scale surface h_s (that rides on the large scale surface).

Thus (Bahar et al, 1982)

$$\langle \sigma^{PQ} \rangle_R = 4k_0^2 \sum_{m=1}^{\infty} \left(\frac{|D^{PQ} \chi^s(\bar{v}_y)|^2}{\bar{n} \cdot \bar{a}_y} \right) \left(\frac{v_y}{2} \right)^{2m} \frac{W_m(v_x, v_z)}{m!} \quad (2.13)$$

$$\cdot P_2(\bar{n}^{-f}, \bar{n}^{-1} | \bar{n}) p(n) dh_x dh_z = \sum_{m=1}^{\infty} \langle \sigma^{PQ} \rangle_{Rm} \quad (2.13)$$

In (2.13) W_m is the two dimensional Fourier transform

$$\begin{aligned} \frac{W_m(v_x, v_z)}{2^{2m}} &= \frac{1}{2\pi^2} \int \langle h_1 h_1' \rangle^m \exp(iv_x \bar{x}_d + iv_z \bar{z}_d) d\bar{x}_d d\bar{z}_d \\ &= \frac{1}{2^{2m}} \int W_{m-1}(v_x', v_z') W_1(v_x - v_x', v_z - v_z') dv_x' dv_z' \\ &= \frac{1}{2^{2m}} W_{m-1}(v_x, v_z) \otimes W_1(v_x, v_z) \end{aligned} \quad (2.14)$$

where the symbol \otimes denotes the two dimensional convolution of W_{m-1} with W_1 , the surface height spectral density function for the small scale surface h_s . Thus

$$W_1(v_x, v_z) = \begin{cases} W(v_x, v_z) & \text{for } k > k_d \\ 0 & \text{for } k \leq k_d \end{cases} \quad (2.15)$$

and v_x and v_z are the orthogonal components of the vector \bar{v} (2.2) tangent to the surface $h_\ell(x, z)$ while v_y is the component of \bar{v} normal to the surface h_ℓ . Thus \bar{v} in the local coordinate system associated with the rough surface h_ℓ can be expressed as (see Fig. 2)

$$\bar{v} = v_x \bar{n}_1 + v_y \bar{n}_2 + v_z \bar{n}_3 \quad (2.16a)$$

where

$$\bar{n}_1 = (\bar{n} \times \bar{a}_z) / |\bar{n} \times \bar{a}_z|, \quad \bar{n}_2 = \bar{n}, \quad \bar{n}_3 = \bar{n}_1 \times \bar{n} \quad (2.16b)$$

and

$$v_x = \bar{v} \cdot \bar{n}_1, \quad v_y = \bar{v} \cdot \bar{n}_2, \quad v_z = \bar{v} \cdot \bar{n}_3 \quad (2.16c)$$

Using the full wave approach it is shown that a suitable value for k_d (the wavenumber where spectral splitting is assumed to occur) is obtained by setting $\beta = 4k_0^2 \langle h_s^2 \rangle = 1.0$ since for this value of β the assumed condition for deep phase modulation is satisfied. For $\beta \geq 1.0$ the total scattering cross section (2.7) is insensitive to variations in the value of k_d (Bahar et al 1982). However, since k_d decreases as β increases, it is necessary to evaluate more terms in (2.13) for larger values of β .

3. Non-Gaussian Joint Probability Density Functions for the Large Scale Surface Heights and the Associated Slope Distribution Function

The principal purpose of this work is to apply the full wave approach to scattering from rough surfaces to surfaces with non-Gaussian surface height distribution functions and to compare the results with these for Gaussian surfaces. In his recent work, Brown (1982) investigates scattering by surfaces for which decorrelation does not imply statistical independence. In this work Brown concludes that the appearance of a specular term coupled with the lack of any experimental scattering data supporting this result "suggests that decorrelation does indeed imply statistical independence for real surfaces."

Thus, even though from a mathematical point of view, statistical independence is not, in general, implied by a lack of correlation (Papoulis 1965), it is assumed in this work that the joint surface height distribution function becomes statistically independent as the surface height decorrelates. Beckmann (1973a,b) derives a method for finding the joint distribution function for the surface height, $f(h, h'; r_d)$, from a given marginal $p(h)$ that is not necessarily normal and a given correlation coefficient $R(r_d)$.

Thus following Beckmann[†] (1973a,b) $f(h,h';r_d)$ is expressed as follows

$$f(h,h';r_d) = p(h)p(h') \sum_{n=0}^{\infty} \frac{R^n(r_d)}{q_n^2} Q_n(h)Q_n(h') \quad (3.1)$$

where the identical functions $p(h)$ and $p(h')$ are the marginals satisfying

$$\int f(h,h';r_d)dh' = p(h) , \quad \int f(h,h';r_d)dh = p(h') \quad (3.2)$$

From (3.2) it also follows that

$$\int f(h,h';r_d)dhdh' = 1 \quad (3.3)$$

In (3.1) it is assumed that the given surface height density function is transformed into a density $p(h)$ which is proportional to the weighting function of a classical set of orthogonal polynomials $Q_n(h)$, i.e.,

$$\int p(h)Q_n(h)Q_m(h)dh = \begin{cases} 0 & n \neq m \\ \frac{2}{q_n} & n = m \end{cases} \quad (3.4)$$

where all q_n are positive and

$$Q_0 = 1 \quad (3.5)$$

thus $q_0 = 1$. Beckmann (1973a) shows that

$$f(h,h';r_d) = \sum_{n=0}^{\infty} \frac{R^n(r_d)}{q_n^2} Q_n(h)Q_n(h') \geq 0 \quad (3.6)$$

thus

$$f(h,h';r_d) \geq 0 \quad (3.7)$$

throughout the domain $a \leq h,h' \leq b$ (where the orthogonality interval of the polynomials Q_n is a,b (3.4)). Furthermore, it can be shown that

[†]For the convenience of the reader, Beckmann's principal results are summarized here. Since there are several errors in the published results, corrected equations are denoted here by the symbol * next to the equation number.

$$\begin{aligned} \langle hh' \rangle &= \iint hh' f(h, h'; r_d) dh dh' = \sum_{n=0}^{\infty} \frac{R^n(r_d)}{q_n^2} \left[\int hp(h) Q_n(h) dh \right]^2 \\ &= R(r_d) (\langle h^2 \rangle - \langle h \rangle^2) + \langle h \rangle^2 \end{aligned} \quad (3.8)$$

in agreement with the condition $f(h, h'; r_d)$ must fulfill if it is to be a two dimensional density of a random process with given correlation coefficient $R(r_d)$. In addition (3.1) clearly satisfies

$$\lim_{r_d \rightarrow \infty} f(h, h'; r_d) \rightarrow p(h)p(h') \quad (3.9)$$

Finally express the function $g(h)$ as follows in an infinite series of orthogonal polynomials

$$g(h) = \sum_{n=0}^{\infty} \alpha_n Q_n(h) \quad (3.10)$$

where on using (3.4) the constant α_n is

$$\alpha_n = \int g(h') p(h') Q_n(h') dh' / q_n^2 \quad (3.11)$$

On interchanging integration on summation (3.10) can be written as

$$g(h) = \int g(h') [p(h') \sum_{n=0}^{\infty} \frac{1}{2} Q_n(h) Q_n(h')] dh' \quad (3.12)$$

thus the quantity in square brackets is the Dirac delta function $\delta(h-h')$.

Thus from (3.1) it follows that

$$\lim_{r_d \rightarrow 0} f(h, h'; r_d) = p(h)\delta(h-h') = p(h')\delta(h-h') \quad *(3.13)$$

On integrating (3.13) with respect to h and h' it is readily shown to satisfy (3.3). (Contrary to the statements by Beckmann (1973a,b), the Dirac delta function does not remain unchanged when multiplied by $p(h)$ and $\lim_{r_d \rightarrow 0} f(h, h'; r_d) \neq \delta(h-h')$). In Beckmann's work (1973a,b), the orthogonal polynomials $Q_n(h)$ can be the Hermite polynomials, the generalized Laguerre polynomials or the

Jacobi polynomials. However, in this work it is assumed for convenience that Q_n are the generalized Laguerre polynomials (Abramowitz and Stegun (1964))

$$Q_n(h) = L_n^{(k-1)}(h) \quad (3.14)$$

Since the weighting functions associated with the Laguerre polynomials are proportional to the gamma functions, the marginals for the large scale surface height probability density functions are the gamma distributions

$$p(h) = \frac{v^k h^{k-1} e^{-vh}}{(k-1)!}, \quad h \geq 0 \quad (3.15)$$

for which the mean is $\langle h \rangle = k/v$, the variance is $\sigma^2 = k/v^2$ and the normalization constant q_n^2 (3.4) is

$$q_n^2 = (k + n-1)! / (k-1)! n! \quad *(3.16)$$

For $k = 1$ (3.15) reduces to the exponential distribution

$$p(h) = v e^{-vh}, \quad (k=1) \quad (3.17)$$

and for the limiting case $k \rightarrow \infty$ (3.15) reduces to the Gaussian distribution by virtue of the Central Limit Theorem. (For most practical purposes $k \geq 25$ is sufficiently close to the limiting case).

$$p(h) = \frac{1}{\sigma\sqrt{2\pi}} \exp \left[-\frac{(h-\langle h \rangle)^2}{2\sigma^2} \right], \quad (k \rightarrow \infty) \quad (3.18)$$

where σ^2 is the variance and $\langle h \rangle$ is the mean height.

Thus using the gamma distribution (3.15), it is sufficient to vary one parameter k to examine the effects of changing the marginal height distribution from exponential to normal in gradual steps.

Following the procedures outlined above, the joint distribution for the surface heights whose marginals are $p(h)$ (3.15) (with $v = 1$ and variance k can be shown to be given by (Beckmann 1973b))

$$f(h, h'; r_d) = \frac{(hh')^{k-1} e^{-(h+h')}}{[(k-1)!]} \sum_{n=0}^{\infty} \frac{R^n (r_d)^n}{(k+n-1)!} L_n^{k-1}(h) L_n^{k-1}(h') \quad (3.19)$$

in which $L_n^{k-1}(h)$ are Laguerre orthogonal polynomials (Abramowitz and Stegun 1964). The corresponding (one dimensional) slope distribution function $p(h_x)$ can be obtained from the inverse Fourier transform

$$p(h_x) = \lim_{r_d \rightarrow 0} \frac{r_d}{2} \int \sum_{n=0}^{\infty} \frac{R^n (r_d)^n}{q_n^2} \int p(h) L_n^{k-1}(h) \exp(iwh) \exp(-ir_d h_x w) dw \quad (3.20)$$

where

$$\sum_{n=0}^{\infty} \frac{R^n}{q_n^2} \left| \int p(h) L_n^{k-1}(h) \exp(iwh) dh \right|^2 = \sum_{n=0}^{\infty} \frac{(n+k-1)! w^{2n} R^n}{n! (1+w^2)^{k+n} (k-1)!} = \frac{1}{[1 + (1-R)w^2]^k} \quad *(3.21)$$

Thus

$$p(h_x) = \lim_{r_d \rightarrow 0} \frac{r_d}{2\pi} \int_{-\infty}^{\infty} \frac{\exp(-iwh_x) dw}{(1 + w^2/w_0^2)^k} \quad (3.22a)$$

where the k^{th} order poles are at points

$$w_{\pm} = \pm i/\sqrt{1-R} = \pm i w_0 \quad (3.22b)$$

Using standard procedures for integration in the complex w plane, the path along the real axis is closed by an infinite semicircle in the lower or upper half plane depending on whether $z > 0$ or $z < 0$. Thus the pole enclosed by the contour is at

$$w = \begin{cases} w_- = -i w_0, & \text{for } z > 0 \\ w_+ = i w_0, & \text{for } z < 0 \end{cases} \quad *(3.23)$$

and (3.22) reduces to

$$p(h_x) = \frac{\gamma e^{-\gamma|h_x|}}{2^{2k-1} (k-1)!} \sum_{j=0}^{k-1} \frac{(2k-j-2)! (2\gamma|h_x|)^j}{j! (k-j-1)!} \quad *(3.24)$$

where

$$\gamma = \lim_{r_d \rightarrow 0} r_d w_0 = \lim_{r_d \rightarrow 0} r_d / \sqrt{1-R} \quad (3.25)$$

For a stationary random process, the correlation function is an even function of r_d (Beckmann 1968) and for small r_d

$$R(r_d) = 1 - \frac{\sigma_x^2}{2\sigma^2} r_d^2 + O(r_d^4) \quad (3.26)$$

where σ_x^2 is the mean square slope

$$\sigma_x^2 = -\sigma^2 R''(0) \quad (3.27)$$

Therefore (3.25) reduces to

$$\gamma = \frac{\sqrt{2} \sigma}{\sigma_x} = \frac{\sqrt{2k}}{\sigma_x}, \quad (v=1) \quad *(3.28)$$

and the slope distribution function corresponding to the two dimensional gamma (surface height) distribution (3.19) is

$$p(h_x) = \frac{2\sqrt{2k} \exp(-\sqrt{2k}|h_x|/\sigma_x)}{\sigma_x 2^{2k} (k-1)!} \sum_{j=0}^{k-1} \frac{(2k-j-2)!}{j! (k-j-1)!} (2\sqrt{2k}|h_x|/\sigma_x)^j \quad *(3.29)$$

The above result can be shown to hold for arbitrary values of v and not just $v = 1$ (Beckmann 1973a). It is assumed in this work that the probability density for the slopes h_x and h_z are independent (as for the Gaussian case Barrick 1970, Brown 1978, Bahar 1981a,b), thus the two dimensional slope distribution for the large scale surface is

$$p(\bar{n}) = p(h_x, h_z) = p(h_x) p(h_z) \quad (3.30)$$

in which $p(h_x)$ and $p(h_z)$ are the same functions as in (3.29). The corresponding slope distribution function is

$$p(h_x) = \frac{1}{\sqrt{2\pi} \sigma_x} \exp(-h_x^2/2\sigma_x^2) \quad (3.31)$$

4. The Explicit Expression for the Shadow Functions Associated with the Non-Gaussian Surface Height Distribution Functions

In this section explicit expressions are derived for the shadow functions related to the non-Gaussian surface height distribution functions considered in Section 3. Brown (1980) recently developed a very convenient procedure to evaluate the shadow functions for surfaces with non-Gaussian height distribution. Following Smith's work (1967), Brown (1980) assumes that the surface heights h and slopes h_x at points separated by the distance r_d are uncorrelated. In addition Brown assumes that decorrelation implies statistical independence. Thus keeping the notation used in this paper, the shadow function for backscatter ($\bar{n}^i = -\bar{n}^i$), $P_2(-\bar{n}^i, \bar{n}^i | \bar{n})$, is the probability that a point on the rough surface is illuminated by the source (and visible at the observation point) given the value of the slope at that point.

$$P_2(-\bar{n}^i, \bar{n}^i | \bar{n}) = S(-\bar{n}^i \cdot \bar{n}) / [1 + \Gamma^i / \mu^i] \quad (4.1)$$

where $S(-\bar{n}^i \cdot \bar{n})$ is the unit step function. The argument $-\bar{n}^i \cdot \bar{n}$ vanishes when the incident (or backscattered) wave normal is tangent to the surface.

Thus, when the plane of incidence is the x, y plane (see Fig. 1), the argument $(-\bar{n}^i \cdot \bar{n})$ vanishes for

$$\mu^i \equiv \cot \theta_o^i = \partial h / \partial x \equiv h_x \quad (4.2)$$

in which θ_o^i is the angle of incidence (2.26) with respect to the reference surface (the x, z plane). Furthermore, in (4.1)

$$\Gamma^i \equiv \Gamma(\mu^i) = \int_{\mu^i}^{\infty} (h_x - \mu^i) p(h_x) dh_x \quad (4.3)$$

in which $p(h_x)$ is the one dimensional slope distribution function. On substituting the non-Gaussian slope distribution function (3.29) (associated

with the gamma surface height distribution) it can be shown that

$$\Gamma(\mu^i)/\mu^i = \frac{\exp(-\sqrt{2k} \mu^i/\sigma_x)}{2^{2k-1} (k-1)!} \sum_{j=0}^{k-1} \frac{(2k-j-2)!}{(k-j-1)!} 2^j \sum_{r=1}^{j+1} \frac{r(\sqrt{2k} \mu^i/\sigma_x)^{j-r}}{(j+1-r)!} \quad (4.4)$$

The shadow function for the bistatic case, $\bar{n}^f \neq \bar{n}^i$, is (Brown 1980)

$$P_2(\bar{n}^f, \bar{n}^i | \bar{n}) = \begin{cases} \frac{S(\bar{n}^i \cdot \bar{n})}{1 + \Gamma^i/\mu^i}, & \theta_o^i \geq \theta_o^f, \phi^f - \phi^i = \pi \\ \frac{S(\bar{n}^f \cdot \bar{n})}{1 + \Gamma^f/\mu^f}, & \theta_o^f \geq \theta_o^i, \phi^f - \phi^i = \pi \\ \frac{S(\bar{n}^f \cdot \bar{n})S(\bar{n}^i \cdot \bar{n})}{1 + (\Gamma^i/\mu^i) + (\Gamma^f/\mu^f)}, & \text{elsewhere} \end{cases} \quad (4.5)$$

In (4.5)

$$\Gamma^f = \Gamma(\mu^f) \text{ and } \mu^f = \cot \theta_o^f \quad (4.6)$$

where θ_o^f is the scatter angle (2.2c) with respect to the reference plane.

The above expressions (4.5) are also in agreement with Sancer's (1969) results for Gaussian surface height distributions. (In Sancer's published results (1969), the inequality symbols should be reversed, Brown (1980)).

5. Illustrative Examples

In this section the like and depolarized backscatter cross sections are evaluated for several composite models of perfectly conducting rough surfaces with different surface height distribution functions. The surface h_ℓ consisting of the large scale spectral components, $0 \leq k \leq k_d$, is assumed to be characterized by the gamma surface height distribution function (3.15) and the associated non-Gaussian slope distribution function (3.29). For the illustrative examples presented here the parameter k is set equal to 1, 2, 5 and 25 and the limiting case ($k \rightarrow \infty$) is represented by the Gaussian distribution (3.18). Two different total mean square slopes are considered

(a) $\sigma_{\lambda t}^2 = 0.0171$ and (b) $\sigma_{\lambda t}^2 = 0.0564$. The surface h_s consisting of the small scale spectral components, $k \geq k_d$, is characterized by Gaussian surface height distribution functions. The wavenumber k_d where spectral splitting is assumed to occur is determined by setting $\beta = 4k_o^2 \langle h_s^2 \rangle = 1$ (Bahar et al 1982) and the specific form assumed for the surface height spectral density function (2.1) is (Brown 1978)

$$W(k) = \frac{\pi}{2} S(k) = \begin{cases} \frac{2}{\pi} B \frac{k^4}{(k^2 + \kappa^2)^4} & , k \leq k_c \\ 0 & , k > k_c \end{cases} \quad (5.1)$$

In (5.1) $W(k)$ is the spectral density function employed by Rice (1951)

and

$$\begin{aligned} B &= .0046 & (\text{case a}) & ; B = 0.0133 & (\text{case b}) \\ k^2 &= v_x^2 + v_z^2 & (\text{cm})^{-2} & ; k_c = 12 & (\text{cm})^{-1} \\ \kappa &= (335.2 \text{ V}^4)^{-1/4} & (\text{cm})^{-1} & ; v = 4.3 & (\text{m/s}) \end{aligned} \quad (5.2)$$

The wavelength for the electromagnetic wave is

$$\lambda_o = 2 \text{ (cm)} \quad , \quad (k_o = 3.1416 \text{ (cm)}^{-1}) \quad (5.3)$$

The mean square height for the small scale surface h_s is

$$\langle h_s^2 \rangle = \int_0^{2\pi} \int_{k_d}^{k_c} \frac{W(k)}{4} k dk d\phi = \frac{B}{2} \left[\frac{1}{k_d^2} - \frac{1}{k_c^2} \right] \quad (5.4)$$

and the total mean square slope for the large scale surface h_l is (Brown 1978)

$$\sigma_{\lambda t}^2 = \sigma_x^2 + \sigma_z^2 = \int_0^{\pi} \int_0^{k_d} \frac{W(k)}{4} k^3 dk d\phi = \left[-\frac{11}{16} + \ln \left[\frac{k_d^2 + \kappa^2}{\kappa^2} \right] \right] \quad (5.5)$$

in which $\sigma_x^2 = \sigma_z^2$.

In Fig. 3, σ times the one dimensional gamma surface height distributions (3.15) are plotted as functions of h/σ for $k = 1, 2, 5, 25$ together with the Gaussian surface height distribution (with $\langle h \rangle / \sigma = \sqrt{k} = 5$). In Fig. 4, the corresponding one dimensional slope distributions times $\sigma_{lt} = \sqrt{2} \sigma_{lx}$ are plotted as functions of h_x / σ_{lt} . In Fig. 5 the corresponding shadow functions (4.5) are plotted as functions of θ_o^1 for backscatter ($\bar{n}^f = -\bar{n}^i$) (a) $\sigma_{lt}^2 = 0.0171$, (b) $\sigma_{lt}^2 = 0.0564$. As expected the shadow function is smaller for the larger mean slopes. The shadow functions are insensitive to the particular form of the slope density functions considered.

In Figs. 6a,b,c and 7a,b,c, the corresponding like polarized and depolarized total backscatter cross sections (2.7) are plotted as functions of θ_o^1 (a) $\langle \sigma^{VV} \rangle$ (b) $\langle \sigma^{HH} \rangle$ (c) $\langle \sigma^{VH} \rangle = \langle \sigma^{HV} \rangle$ in Figs. 6a,b,c $\sigma_{lt}^2 = 0.0171$ and in Figs. 7a,b,c $\sigma_{lt}^2 = 0.0564$. The like backscatter cross section near normal incidence ($\theta_o \approx 0$) is largest for the case $k = 1$. This is expected since the case $k = 1$ corresponds to a surface with a slope distribution which has the largest zero slope probability. On the other hand consistent with the above results, the depolarized backscatter cross sections near normal incidence are smallest for the case $k = 1$. The backscatter cross section for $k = 25$ is practically indistinguishable from the backscatter for Gaussian random surfaces. Furthermore, as one may expect, the spread in the values for the backscatter cross sections as k varies from 1 through ∞ increases as the mean square slope σ_{lt}^2 increases. At large angles of incidence θ_o^1 , the spread in the values of the like backscatter cross sections is more pronounced for the horizontally polarized waves than for the vertically polarized waves. The reason for this is found

by examining the expression for the dominant term at large angles θ_o^1 , i.e., $\langle \sigma^{PQ} \rangle_{R1}$ (first order Bragg). In this term $|v_y^D{}^{HH}|^2$ is proportional to $|\bar{n}^{-1} \cdot \bar{n}|^4$ while $|v_y^D{}^{VV}|^2$ is proportional to $|2 - (\bar{n}^{-1} \cdot \bar{n})^2|^2$. The latter term is both larger and less sensitive to slope variations $\bar{n}(h_x, h_z)$. In Figs. 8a,b,c,d and 9a,b,c,d, $\langle \sigma^{VV} \rangle_T$ the total backscatter cross sections, $\langle \sigma^{VV} \rangle_o$ the large scale backscatter cross section $\langle \sigma^{VV} \rangle_{R1}$, the leading term of the small scale cross section (which corresponds to first order Bragg scatter) and the remainder term $\langle \sigma^{VV} \rangle_{R2} + \langle \sigma^{VV} \rangle_{R3}$ are plotted as functions of θ_o^1 , case (a) $k = 1$, case (b) $k = 2$, case (c) $k = 5$, case (d) Gaussian surface heights. The results for $k = 25$ are not shown since they are indistinguishable from the results for the Gaussian surface). In Figs. 8a,b,c,d, $\sigma_{lt}^2 = 0.0171$ and in Figs. 9a,b,c,d $\sigma_{lt}^2 = 0.0564$. The corresponding results for σ^{HH} and $\sigma^{HV} = \sigma^{VH}$ are presented in Figs. 10a,b,c,d and 11a,b,c,d, 12a,b,c,d and 13a,b,c,d. From the above plots of the backscatter cross section it is seen that not only is the total backscatter cross section $\langle \sigma^{PQ} \rangle_T$ sensitive to changes in values of k , but the individual terms in the weighted sum (2.7) are also sensitive to changes in k . Furthermore, except for near grazing angles the backscatter cross section for the small scale surface $\langle \sigma^{PQ} \rangle_R$ cannot be approximated by the leading term in the series (2.13) which corresponds to first order Bragg scatter. It has been shown using the full wave approach, Bahar et al. (1982), that the total backscatter cross section $\langle \sigma^{PQ} \rangle_T$ is independent of the specific choice of k_d for $\beta \geq 1$ provided none of the significant terms in (2.13) are neglected. The terms $\langle \sigma \rangle_{Rm}$, for $m \geq 4$, can be neglected for all θ_o when k_d is chosen such that $\beta = 1$.

On the basis of the above results, several schemes can be devised to distinguish between the backscatter cross sections for different values of k .

The behavior of $\langle \sigma^{PP} \rangle_T$ (P=V,H) near normal incidence is of particular interest in this respect. Thus one notices that $\left| \frac{d\langle \sigma^{PP} \rangle}{d\theta_o^1} \right|_{\theta_o^1=0}$ is largest for $k = 1$ and decreases gradually as k increases. Since $\langle \sigma^{HH} \rangle_T$ is more sensitive to variations in k for $\theta_o > 25^\circ$, the backscatter cross sections for horizontally polarized waves are more indicative of the particular form of the rough surfaces height distribution than the backscatter cross sections for the vertically polarized waves. The depolarized backscatter cross sections $\langle \sigma^{PQ} \rangle$ (P≠Q) are rather insensitive to the particular form of the rough surface height distribution except near normal incidence where $\left| \frac{d\langle \sigma^{PQ} \rangle}{d\theta_o} \right|_{\theta_o=0}$ is largest for $k = 1$.

6. Concluding Remarks

Full wave expressions for the like polarized and the depolarized scattering cross sections are derived for a broad family of non-Gaussian rough surfaces. It is assumed that when the surface heights decorrelate they become statistically independent. For the cases considered in the illustrative examples, it is shown that while the shadow functions are not very sensitive to the parameter k ($=1,2,3\dots$) of the surface height probability density assumed, the backscatter cross sections are sensitive to the parameter k .

The like polarized backscatter cross sections $\langle \sigma^{VV} \rangle_T$ and $\langle \sigma^{HH} \rangle_T$ have the same dependence on k for small angles of incidence θ_o^1 , however for large angles θ_o^1 , the cross section $\langle \sigma^{HH} \rangle_T$ is much more sensitive to k than $\langle \sigma^{VV} \rangle_T$. An examination of the expression for the dominant term corresponding to first order Bragg scatter $\langle \sigma^{PP} \rangle_{R1}$ provides an explanation to this phenomenon. The depolarized backscatter cross sections $\langle \sigma^{PQ} \rangle_T$ (P≠Q) are sensitive to k only near normal

incidence. For $\theta_0^i = 0$, the like polarized cross section $\langle \sigma^{PP} \rangle_T$ is largest for the smallest value of k ($k = 1$). This is because the slope probability density for zero slope is largest when $k = 1$. Thus consistent with energy conservation as the like polarized cross section increases with decreasing k values, the depolarized cross section decreases with decreasing k values. Both the total backscatter cross sections and the components of the weighted sum of cross sections are presented in Section 5. The terms corresponding to $\langle \sigma^{PQ} \rangle_{Rm}$ $m \geq 2$ cannot be neglected in this work and a perturbed physical optics approach is not suitable for determining the total backscatter cross section (Bahar et al. 1982).

Acknowledgments

This paper was sponsored by the U.S. Air Force Contract No. F19628-81-K-002J. Figures 3, 4 and 5 were prepared by W. Warnsholz and the manuscript was typed by Mrs. E. Everett.

The authors wish to thank P. Beckmann and D. Barrick for stimulating discussions.

Figure Captions

- Figure 1. Plane of incidence, scattering plane, and reference (x,z) plane.
- Figure 2. Local plane of incidence and scatter and local coordinate system with unit vectors $\bar{n}_1, \bar{n}_2, \bar{n}_3$.
- Figure 3. The one dimensional gamma surface height distributions times σ as functions of h/σ for $k = 1, 2, 5, 25$ together with the Gaussian surface height distribution with $\langle h \rangle / \sigma = 5$.
 (\square) $k = 1$, (Δ) $k = 2$, (+) $k = 5$, (X) $k = 25$, (\diamond) Gaussian.
- Figure 4. The one dimensional slope distributions times $\sigma_{lt} = \sqrt{2} \sigma_x$ as functions of h_x / σ_{lt} , (\square) $k = 1$, (Δ) $k = 2$, (+) $k = 5$, (X) $k = 25$, (\diamond) Gaussian.
- Figure 5. The shadow functions of functions of θ_o^i for backscatter.
 $\sigma_{lt}^2 = 0.0171$ and $\sigma_{lt}^2 = 0.0564$ (\square) $k = 1$, (Δ) $k = 2$, (+) $k = 5$, (X) $k = 25$, (\diamond) Gaussian.
- Figure 6. The total backscatter cross sections (2.7) as functions of θ_o^i for $\sigma_{lt}^2 = 0.0171$
 (a) $\langle \sigma^{VV} \rangle$ (b) $\langle \sigma^{HH} \rangle$ (c) $\langle \sigma^{VH} \rangle = \langle \sigma^{HV} \rangle$.
 (\square) $k = 1$, (Δ) $k = 2$, (+) $k = 5$, (X) $k = 25$, (\diamond) Gaussian.
- Figure 7. The total backscatter cross sections (2.7) as functions of θ_o^i for $\sigma_{lt}^2 = 0.0564$
 (a) $\langle \sigma^{VV} \rangle$ (b) $\langle \sigma^{HH} \rangle$ (c) $\langle \sigma^{VH} \rangle = \langle \sigma^{HV} \rangle$
 (\square) $k = 1$, (Δ) $k = 2$, (+) $k = 5$, (X) $k = 25$, (\diamond) Gaussian.
- Figure 8. Backscatter cross sections $(-)\langle \sigma^{VV} \rangle_T, (X)\langle \sigma^{VV} \rangle_o, (\square)\langle \sigma^{VV} \rangle_{R1}, (\Delta)\langle \sigma^{VV} \rangle_{R2} + \langle \sigma^{VV} \rangle_{R3}$ as functions of θ_o^i for $\sigma_{lt}^2 = 0.0171$
 (a) $k = 1$, (b) $k = 2$, (c) $k = 5$, (d) Gaussian
- Figure 9. Backscatter cross sections $(-)\langle \sigma^{VV} \rangle_T, (X)\langle \sigma^{VV} \rangle_o, (\square)\langle \sigma^{VV} \rangle_{R1}, (\Delta)\langle \sigma^{VV} \rangle_{R2} + \langle \sigma^{VV} \rangle_{R3}$ as functions of θ_o^i for $\sigma_{lt}^2 = 0.0564$
 (a) $k = 1$, (b) $k = 2$, (c) $k = 5$, (d) Gaussian.

Figure 10. Backscatter cross sections $(-)\langle\sigma_{T}^{HH}\rangle$, $(X)\langle\sigma_{O}^{HH}\rangle$, $(\square)\langle\sigma_{R1}^{HH}\rangle$,
 $(\Delta)\langle\sigma_{R2}^{HH}\rangle + \langle\sigma_{R3}^{HH}\rangle$ as functions of θ_{o}^1 for $\sigma_{lt}^2 = 0.0171$

(a) $k = 1$, (b) $k = 2$, (c) $k = 5$, (d) Gaussian

Figure 11. Backscatter cross sections $(-)\langle\sigma_{T}^{HH}\rangle$, $(X)\langle\sigma_{O}^{HH}\rangle$, $(\square)\langle\sigma_{R1}^{HH}\rangle$,
 $(\Delta)\langle\sigma_{R2}^{HH}\rangle + \langle\sigma_{R3}^{HH}\rangle$ as functions of θ_{o}^1 for $\sigma_{lt}^2 = 0.0564$

(a) $k = 1$, (b) $k = 2$, (c) $k = 5$, (d) Gaussian.

Figure 12. Backscatter cross sections $(-)\langle\sigma_{T}^{VH}\rangle$, $(X)\langle\sigma_{O}^{VH}\rangle$, $(\square)\langle\sigma_{R1}^{VH}\rangle$,
 $(\Delta)\langle\sigma_{R2}^{VH}\rangle + \langle\sigma_{R3}^{VH}\rangle$ as functions of θ_{o}^1 for $\sigma_{lt}^2 = 0.0171$

(a) $k = 1$, (b) $k = 2$, (c) $k = 5$, (d) Gaussian.

Figure 13. Backscatter cross sections $(-)\langle\sigma_{T}^{VH}\rangle$, $(X)\langle\sigma_{O}^{VH}\rangle$, $(\square)\langle\sigma_{R1}^{VH}\rangle$,
 $(\Delta)\langle\sigma_{R2}^{VH}\rangle + \langle\sigma_{R3}^{VH}\rangle$ as functions of θ_{o}^1 for $\sigma_{lt}^2 = 0.0564$.

(a) $k = 1$, (b) $k = 2$, (c) $k = 5$, (d) Gaussian.

References

1. Abramowitz, M. and I. A. Stegun (1964). Handbook of Mathematical Tables, Applied Math Ser. 55, National Bureau of Standards, Washington, D.C.
2. Bahar, E. (1981a), "Scattering Cross Sections from Rough Surfaces--Full Wave Analysis," Radio Science, 16(3), pp. 331-341.
3. Bahar, E. (1981b), "Scattering Cross Sections for Composite Random Surfaces--Full Wave Analysis," Radio Science, 16(6), pp. 1327-1335.
4. Bahar, E., D. E. Barrick and M. A. Fitzwater (1982), "Computations of Scattering Cross Sections for Composite Surfaces and the Specification of the Wavenumber Where Spectral Splitting Occurs," (to be published).
5. Barrick, D. E. (1970), Rough Surfaces, in Radar Cross Section Handbook, Chapter 9, Plenum Press, New York.
6. Beckmann, P. (1973), Orthogonal Polynomials for Engineers and Physicists, Boulder, Colo., Golem Press.
7. Beckmann, P. (1973), "Scattering by Non-Gaussian Surfaces," IEEE Transactions on Antennas and Propagation, AP-21(2), pp. 169-175.
8. Brown, G. S. (1978), "Backscattering from a Gaussian-Distributed Perfectly Conducting Rough Surface," IEEE Transactions on Antennas and Propagation, AP-26(3), pp. 472-482.
9. Brown, G. S. (1980), "Correction to Backscattering from a Gaussian-Distributed Perfectly Conducting Rough Surface," IEEE Transactions on Antennas and Propagation, AP-28(6), pp. 943-946.
10. Brown, G. S. (1981), "Scattering from a Class of Randomly Rough Surfaces," Radio Science, Sept.-Oct. 1982, (in press).
11. Papoulis, A. (1965), Probability, Random Variables and Stochastic Processes, McGraw-Hill, New York.
12. Rice, S. O. (1951), "Reflection of Electromagnetic Waves from a Slightly Rough Surface," Communication of Pure and Applied Math, 4, pp. 351-378.
13. Sancer, M. I. (1969), "Shadow-Corrected Electromagnetic Scattering from a Randomly Rough Surface," IEEE Transactions on Antennas and Propagation, AP-17(5), pp. 577-585.
14. Smith, B. G. (1967), "Geometrical Shadowing of a Randomly Rough Surface," IEEE Transactions on Antennas and Propagation, AP-15(5), pp. 668-671.

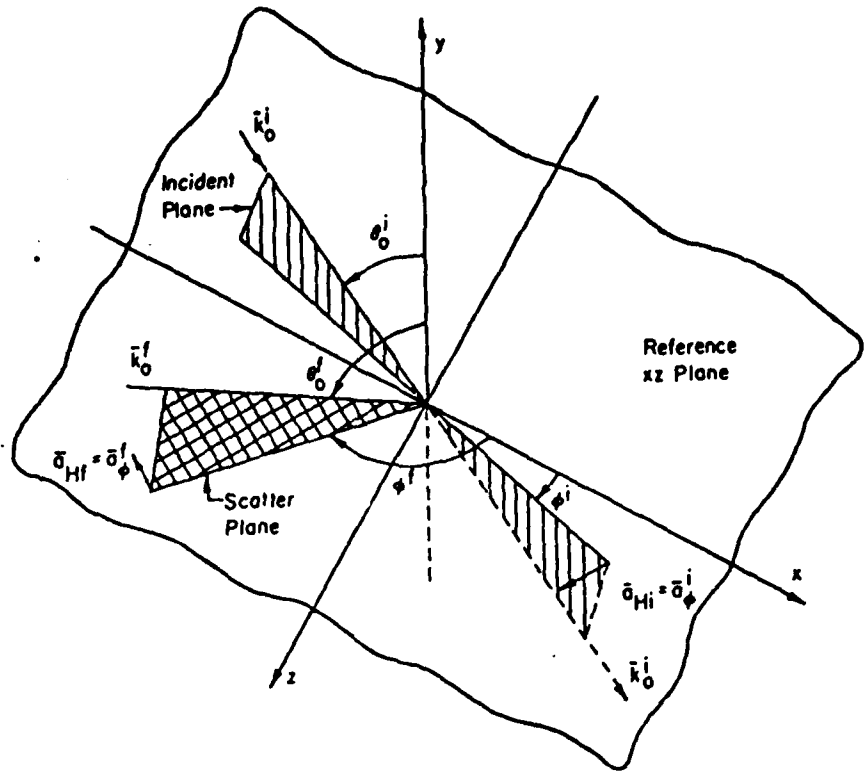


Fig. 1

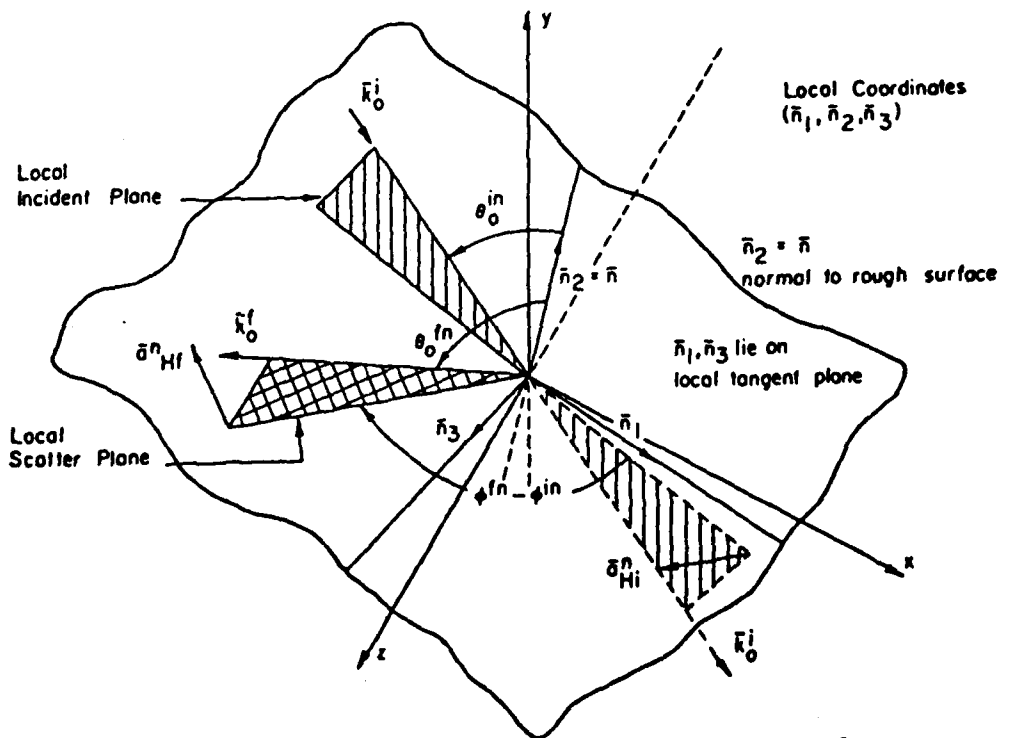


Fig. 2

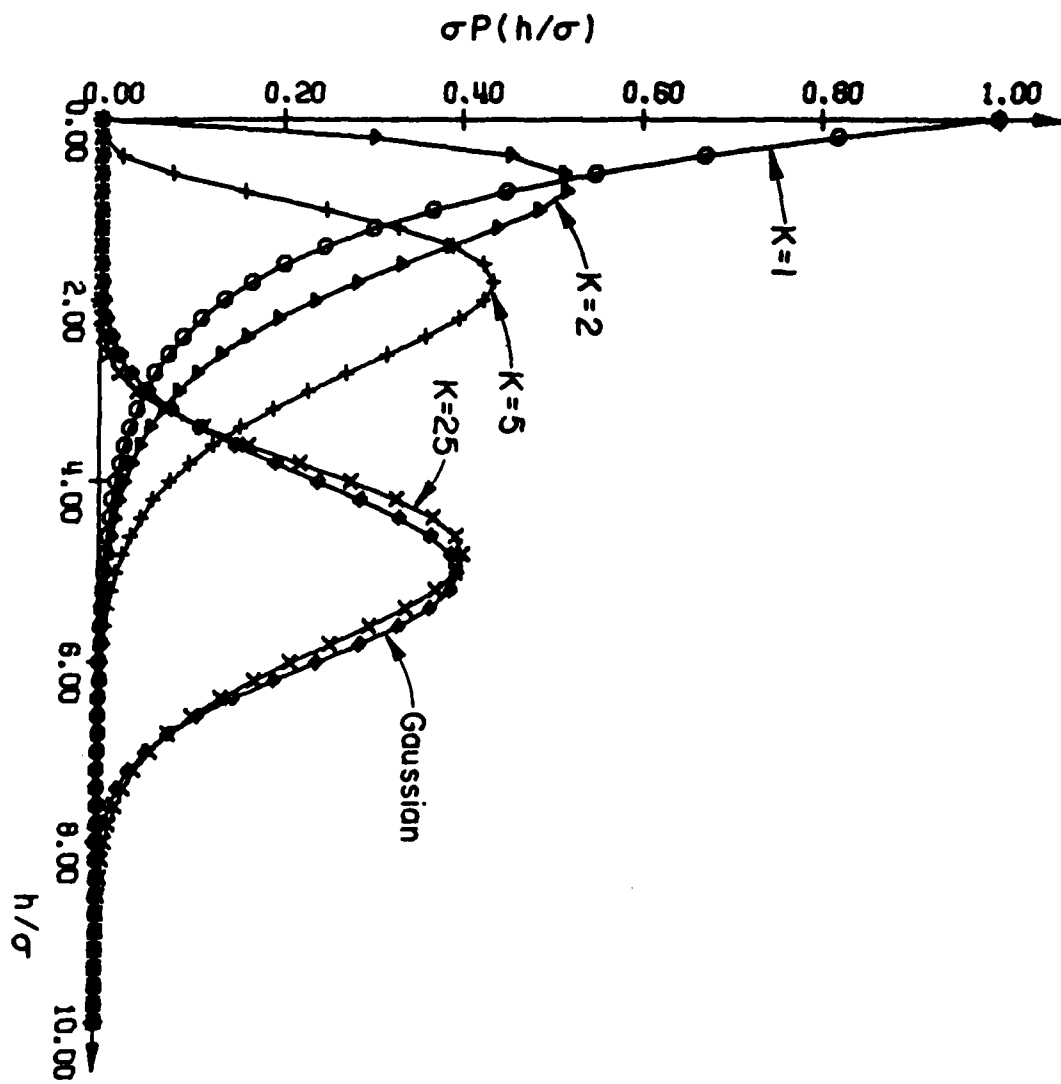


FIG. 3

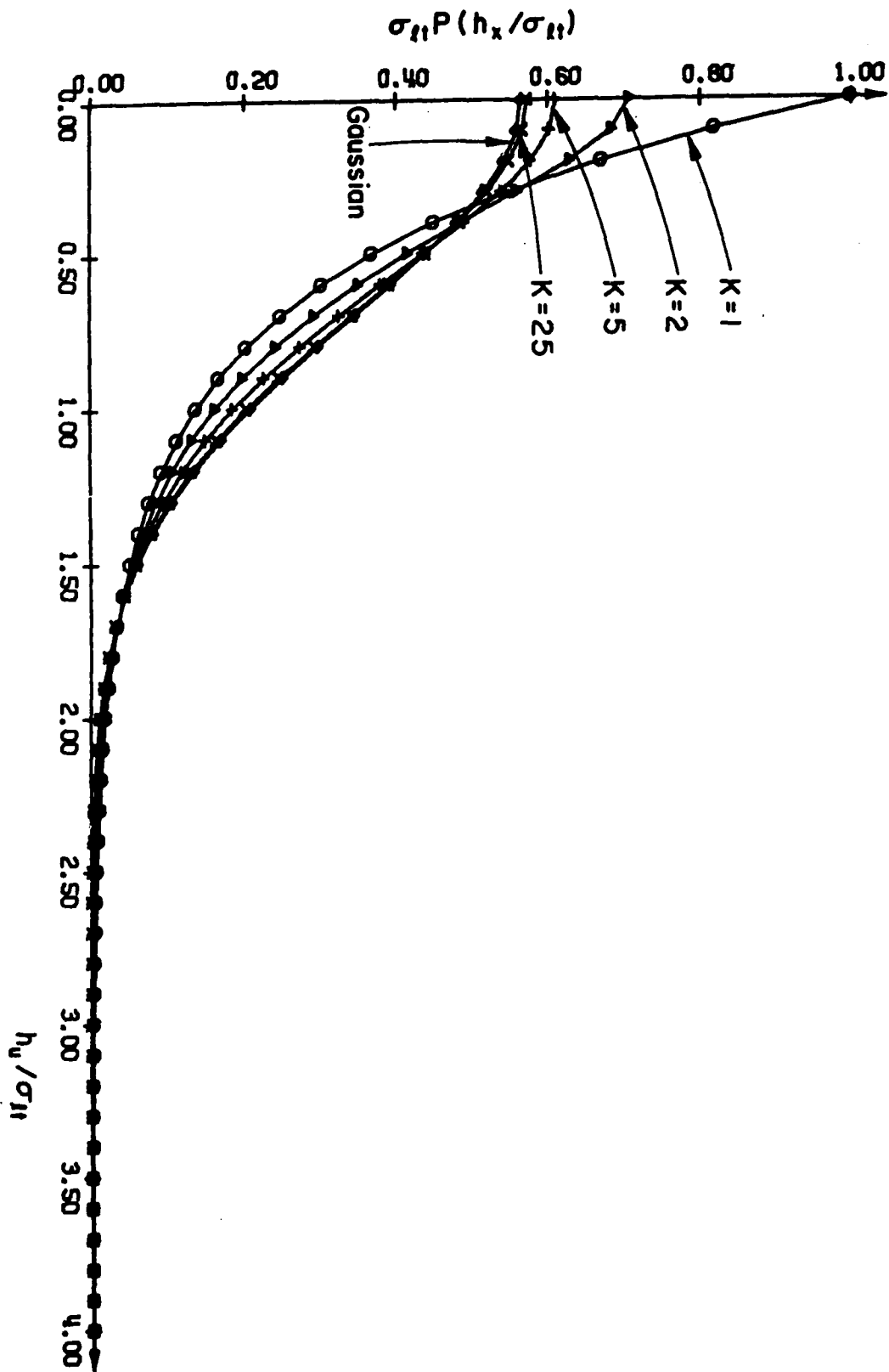


FIG. 4

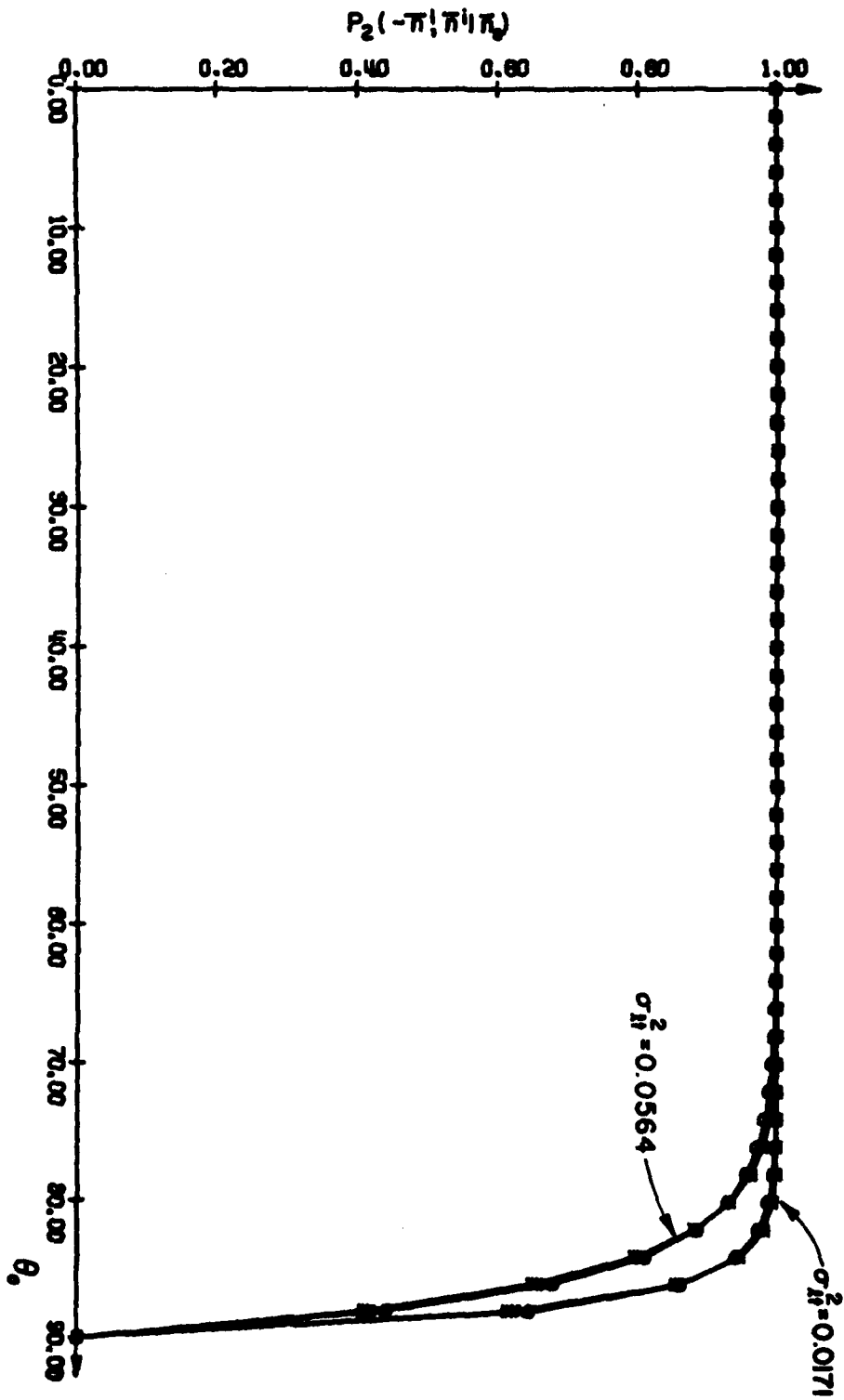


FIG. 5

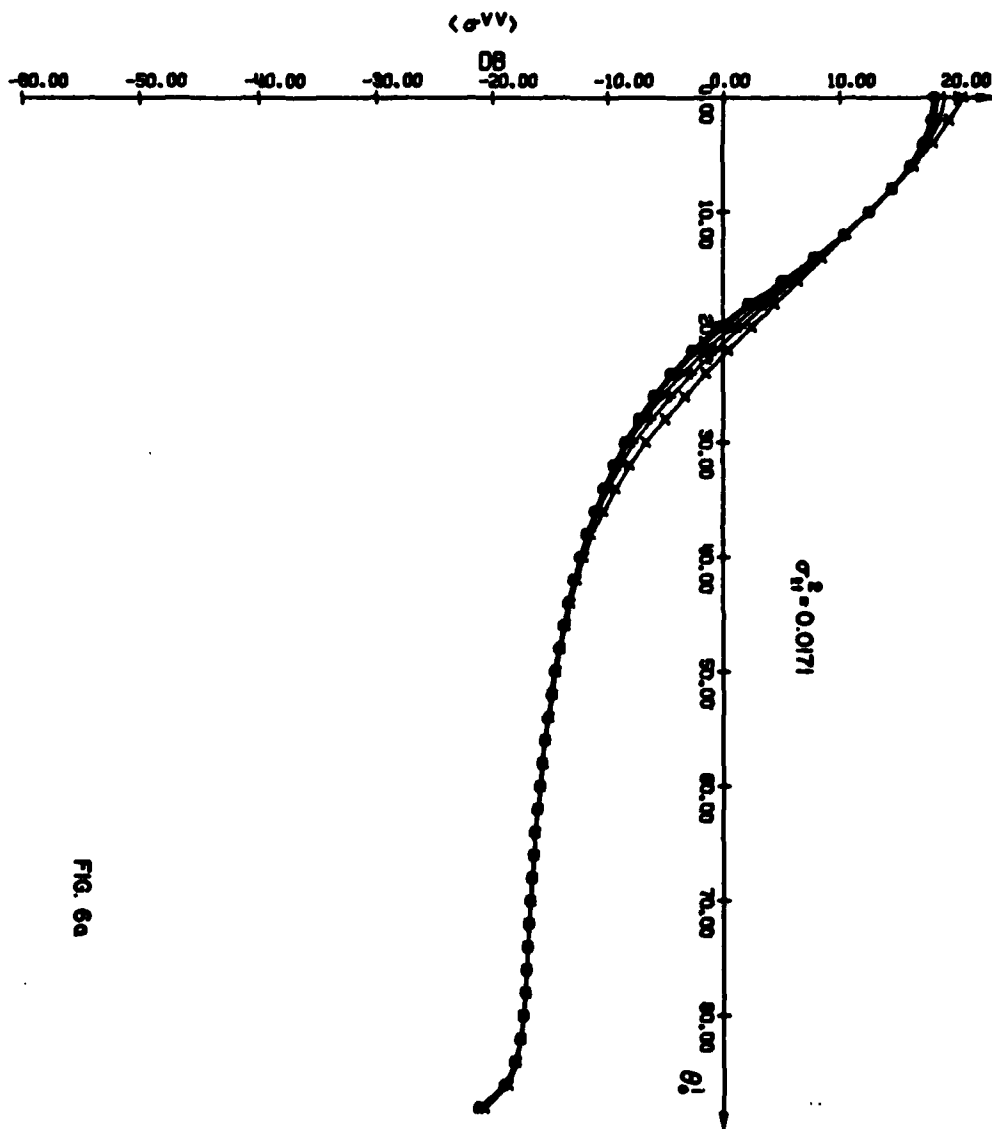


FIG. 6a

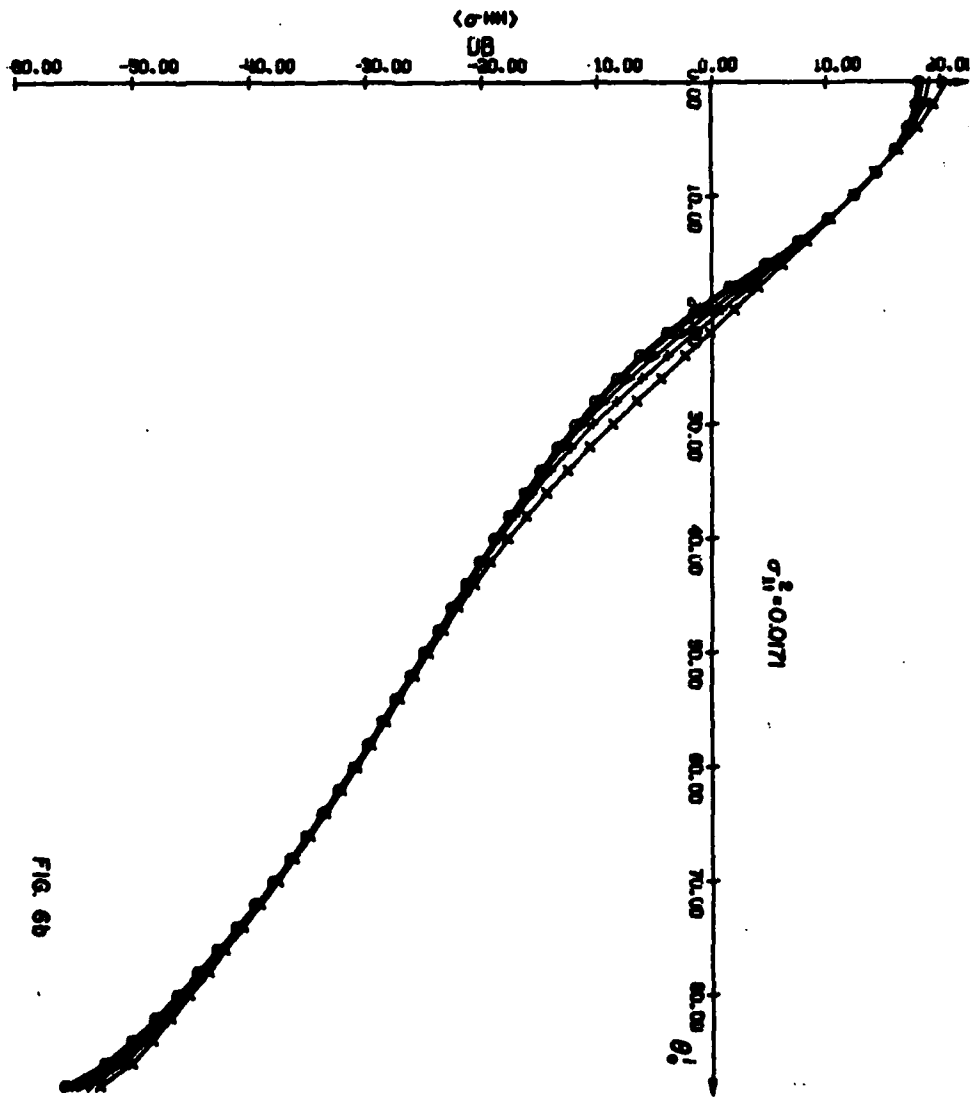


FIG. 6B

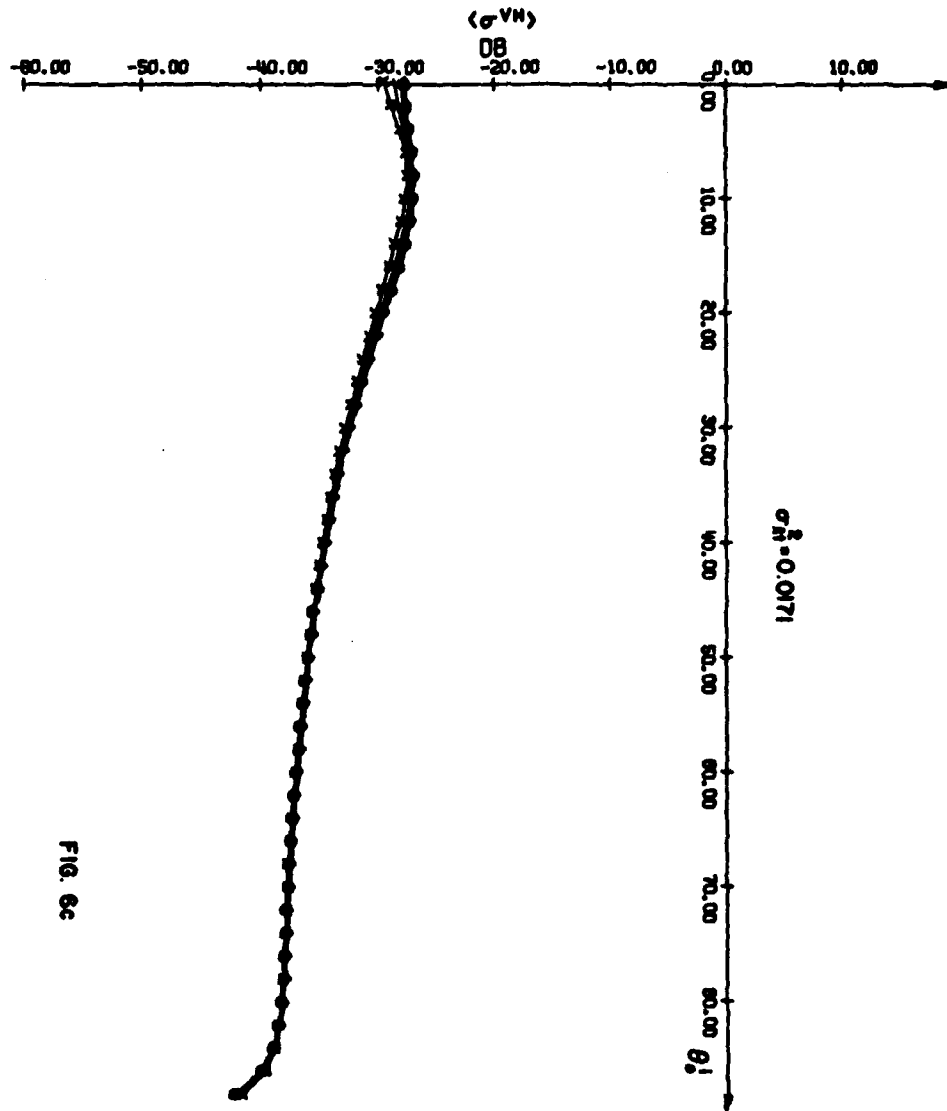


FIG. 6c

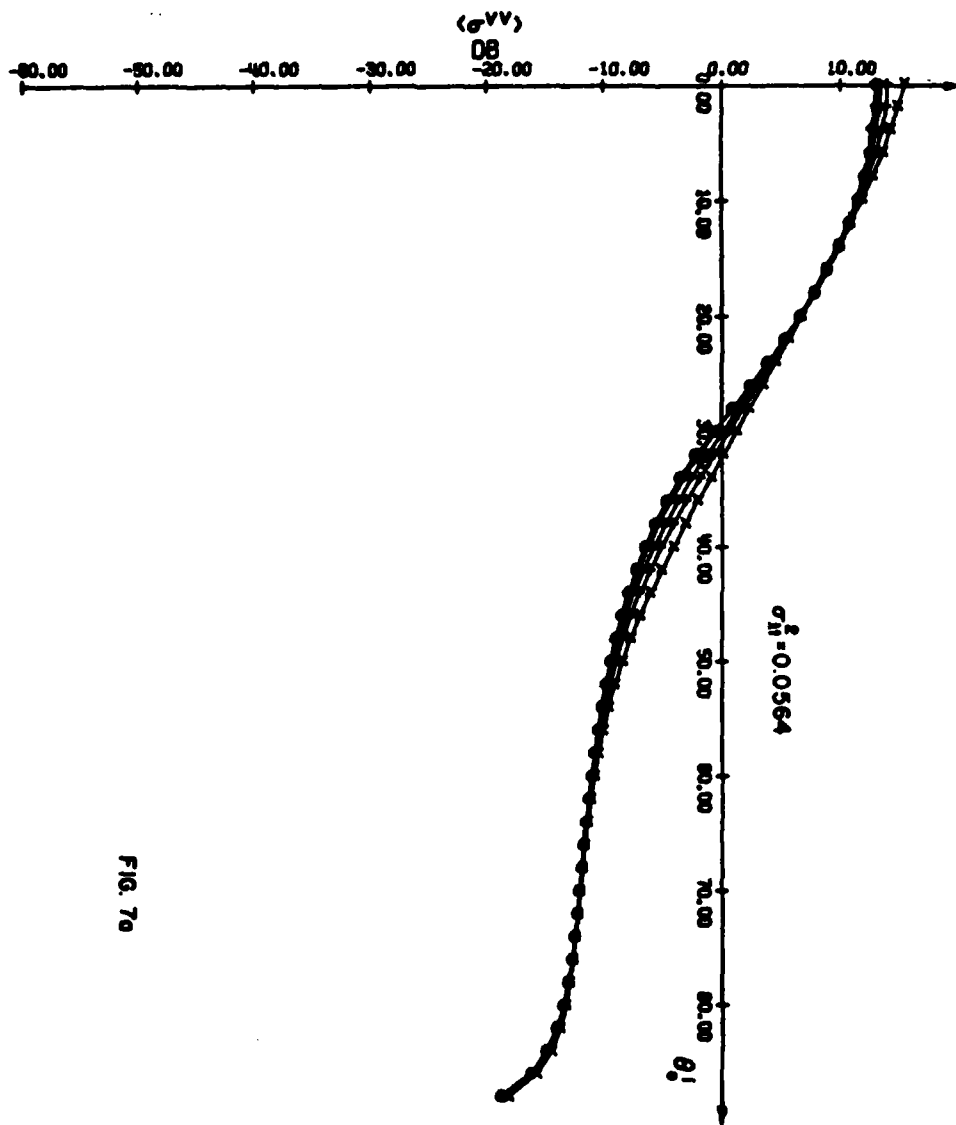


FIG. 70

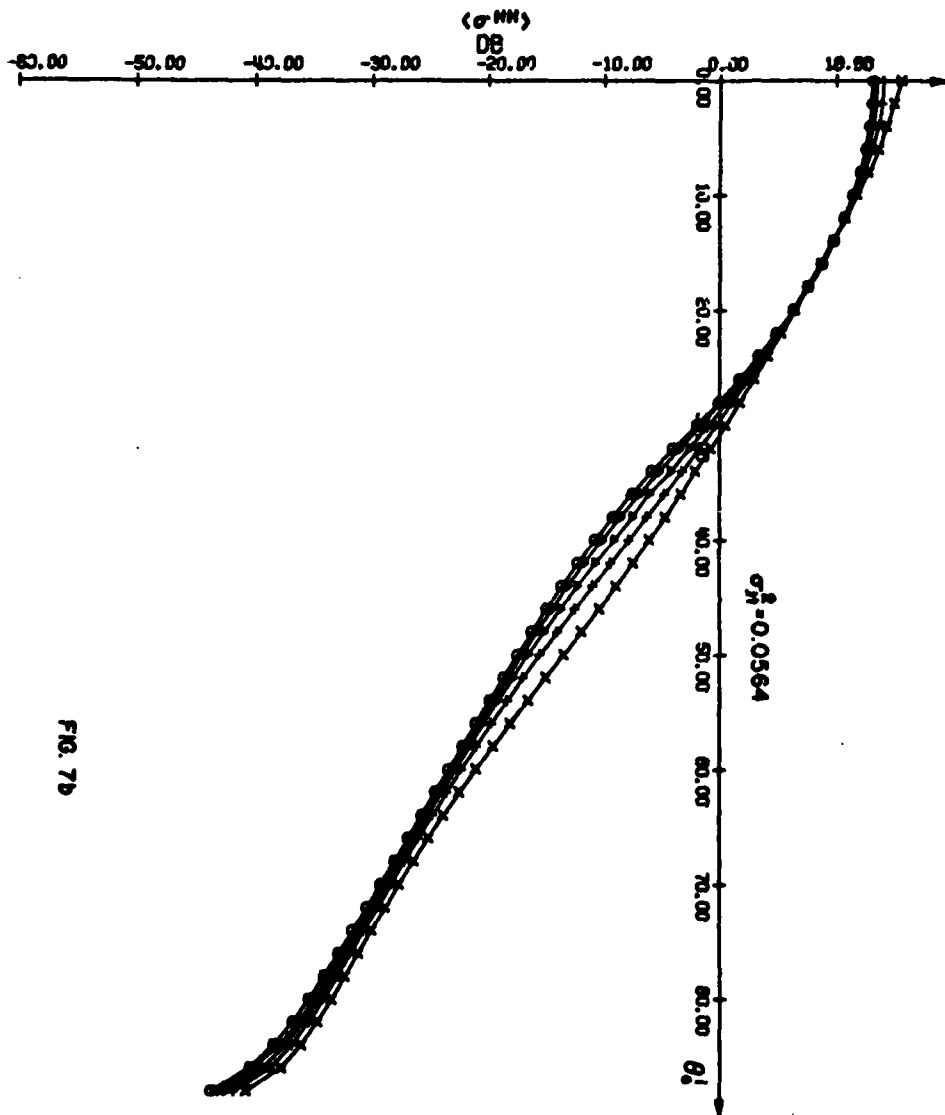


FIG. 7b

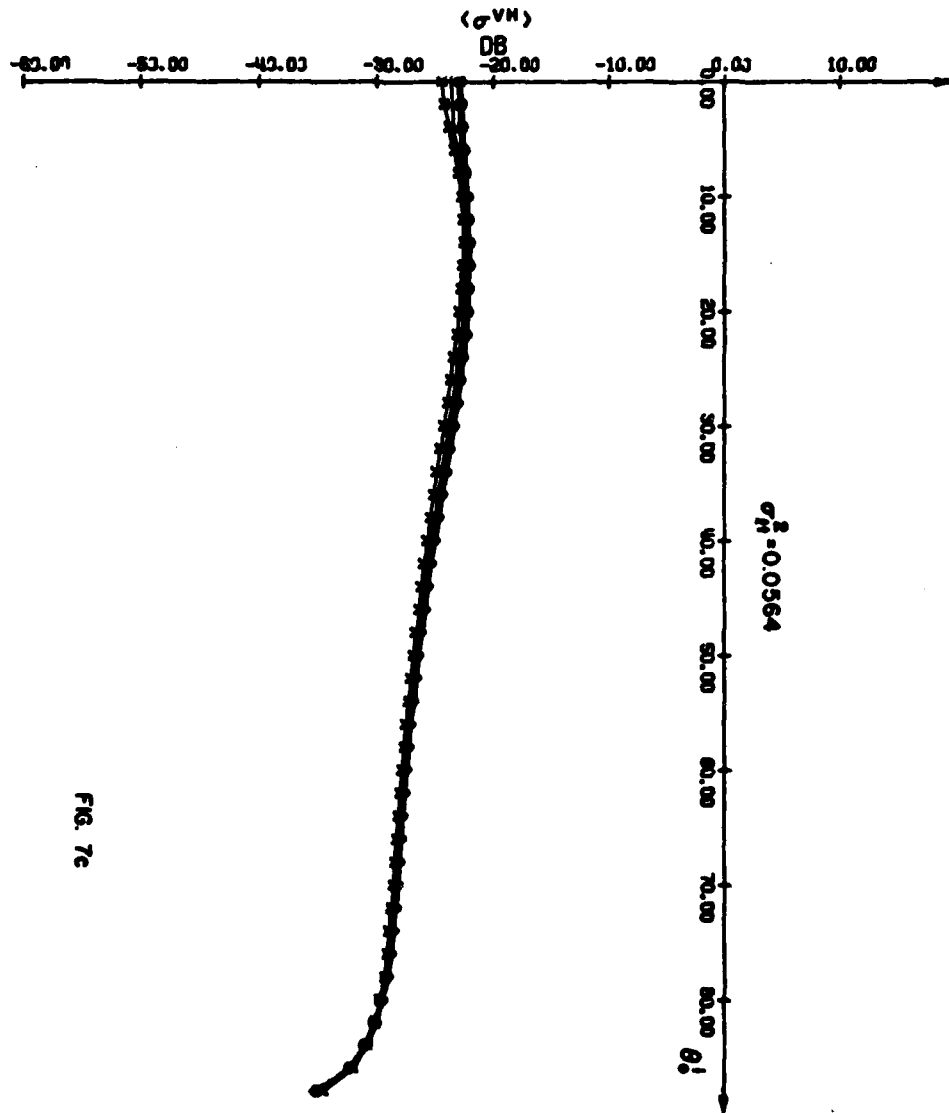


FIG. 7c

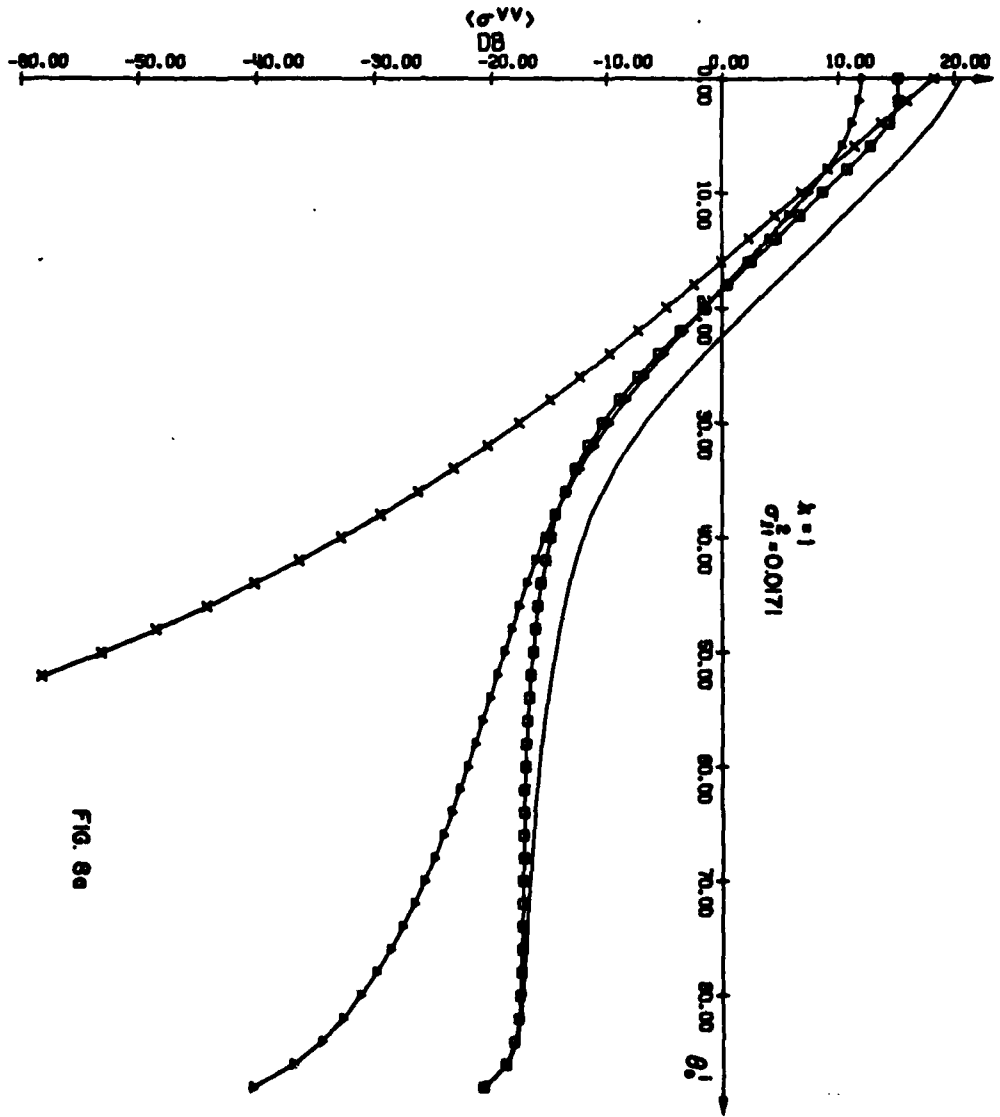


FIG. 8a

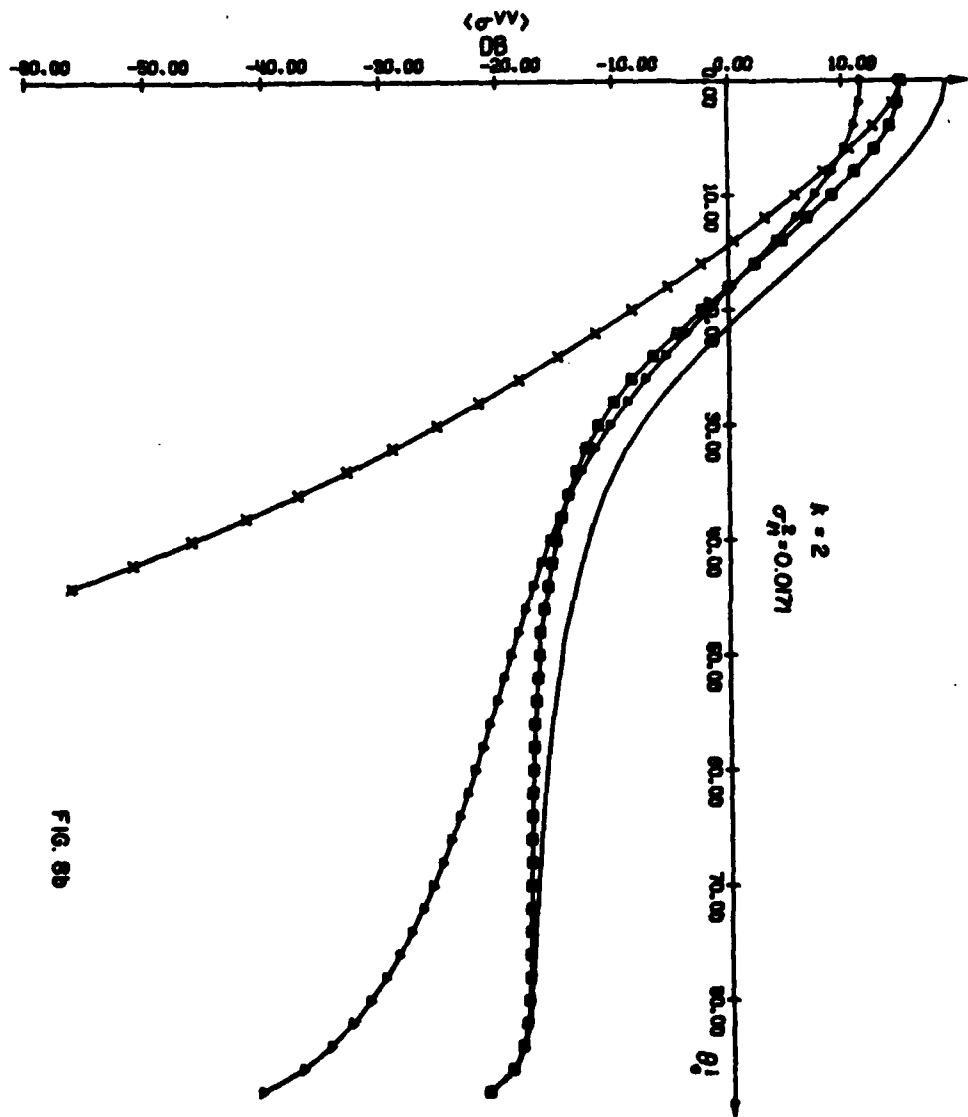


FIG. 8B

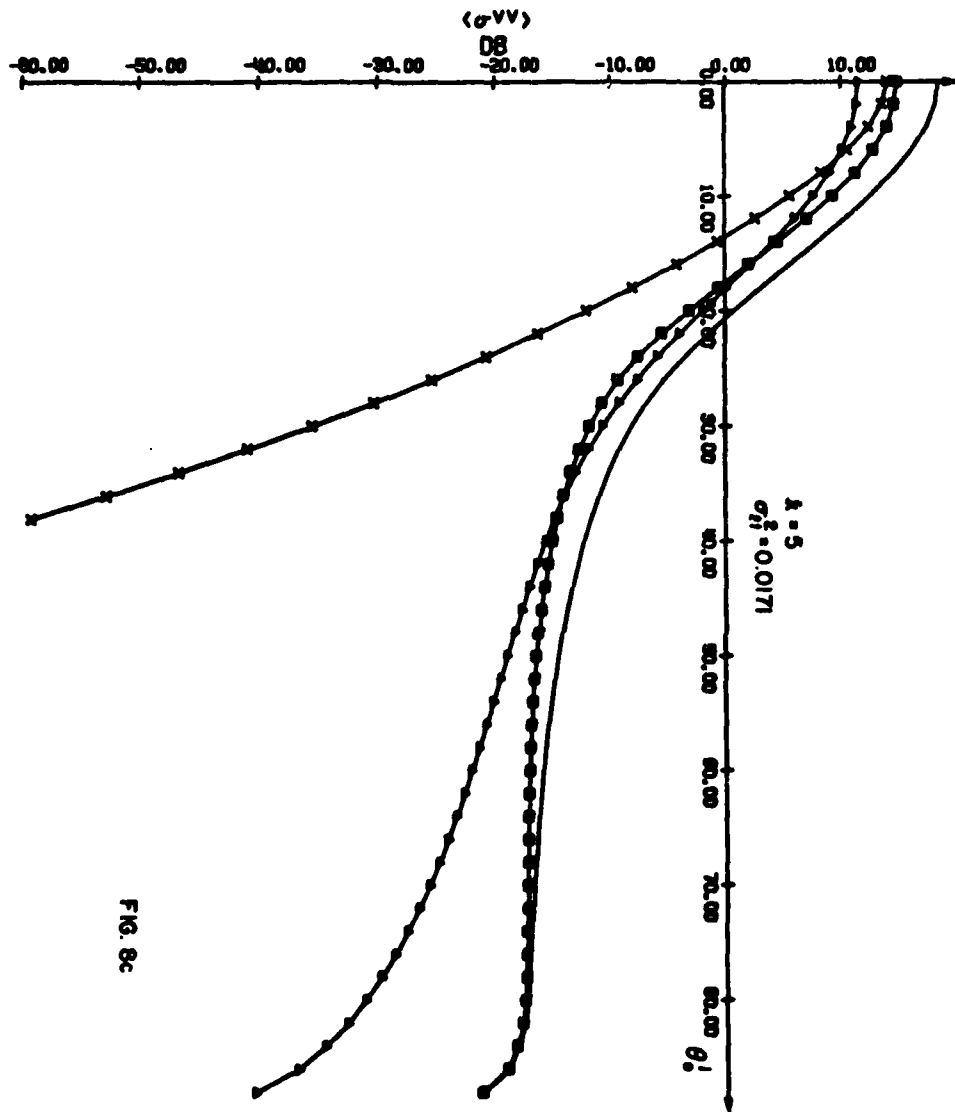


FIG. 8c

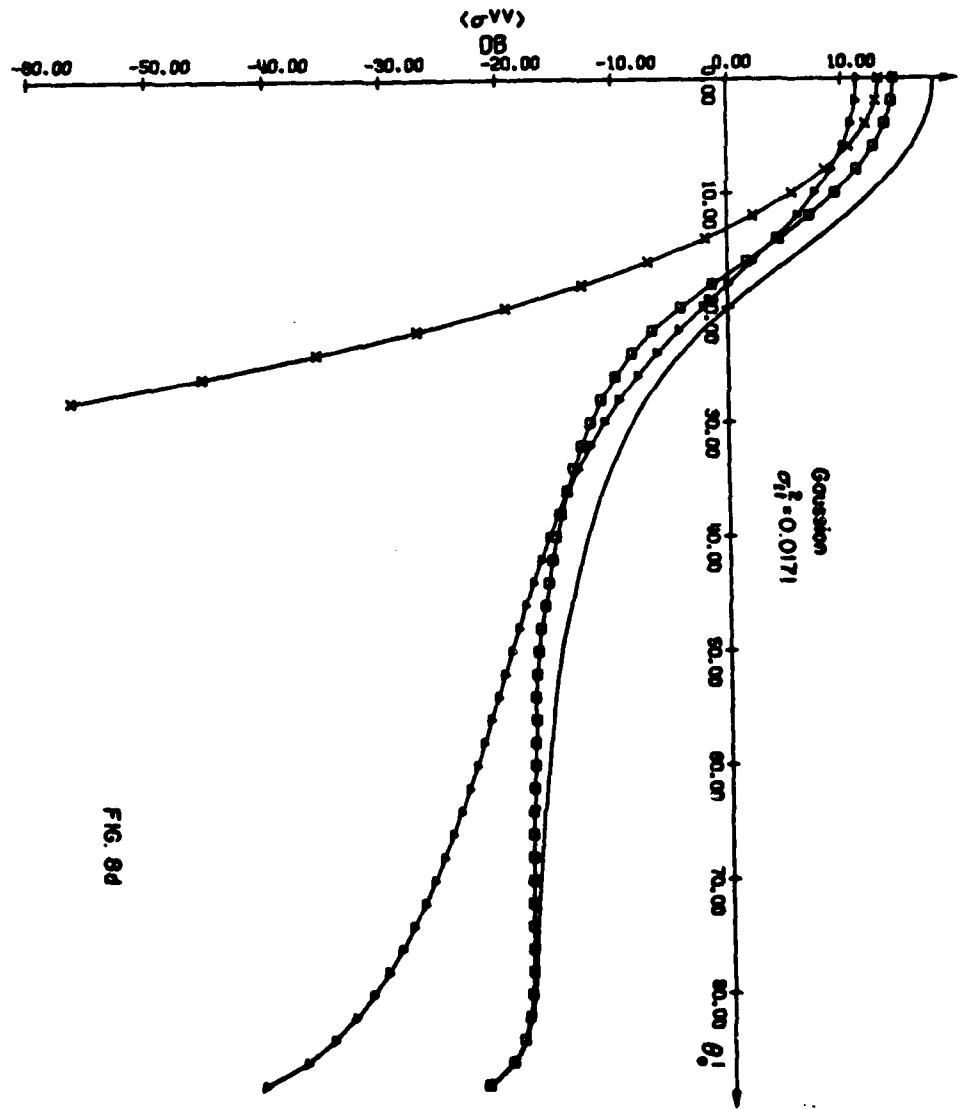


FIG. 84

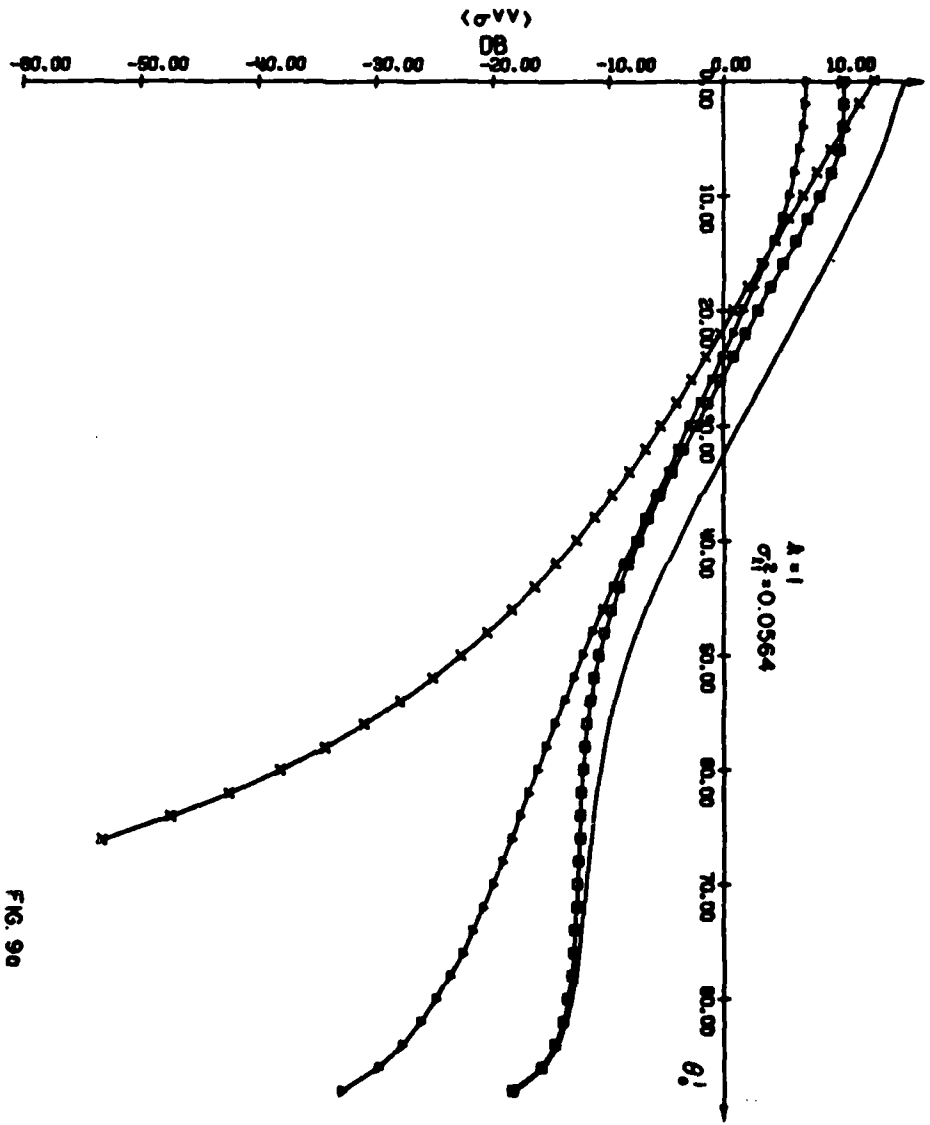


FIG. 9a

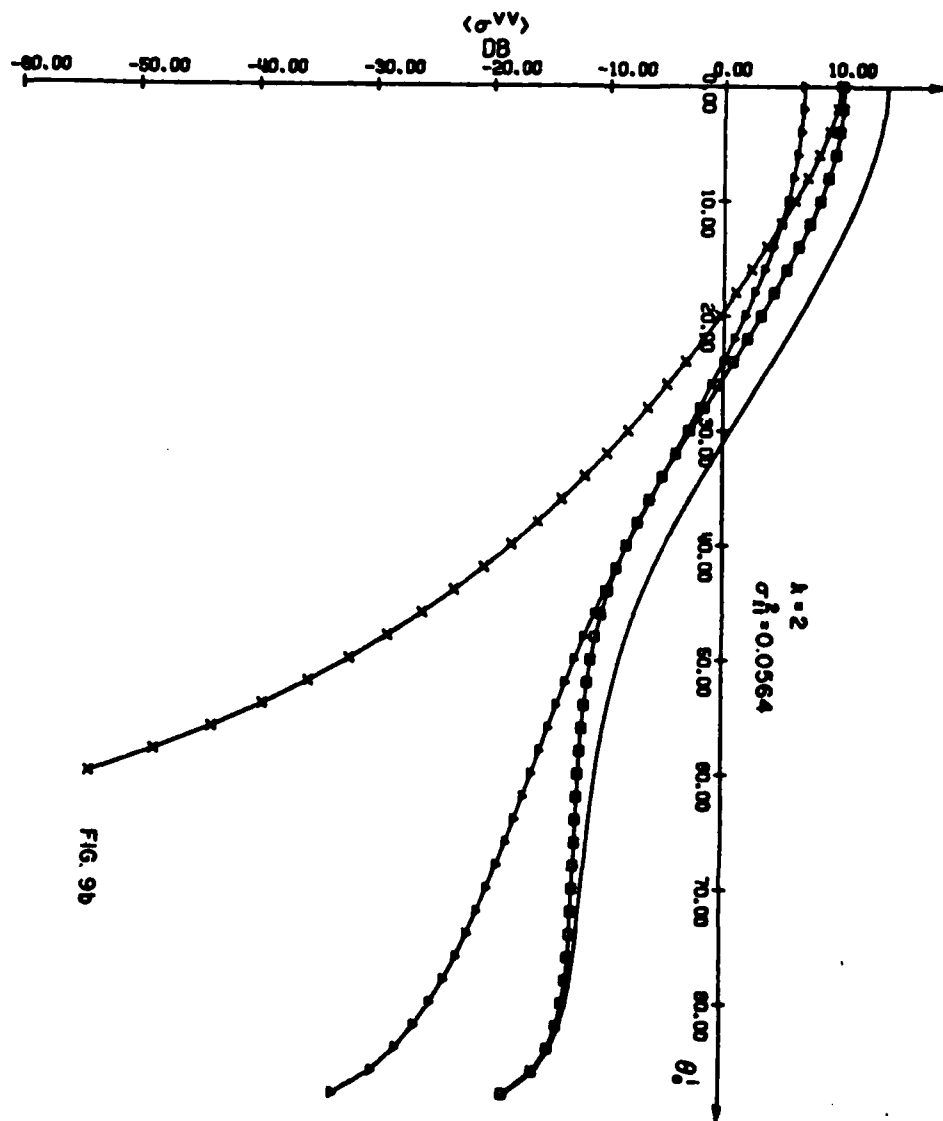


FIG. 9b

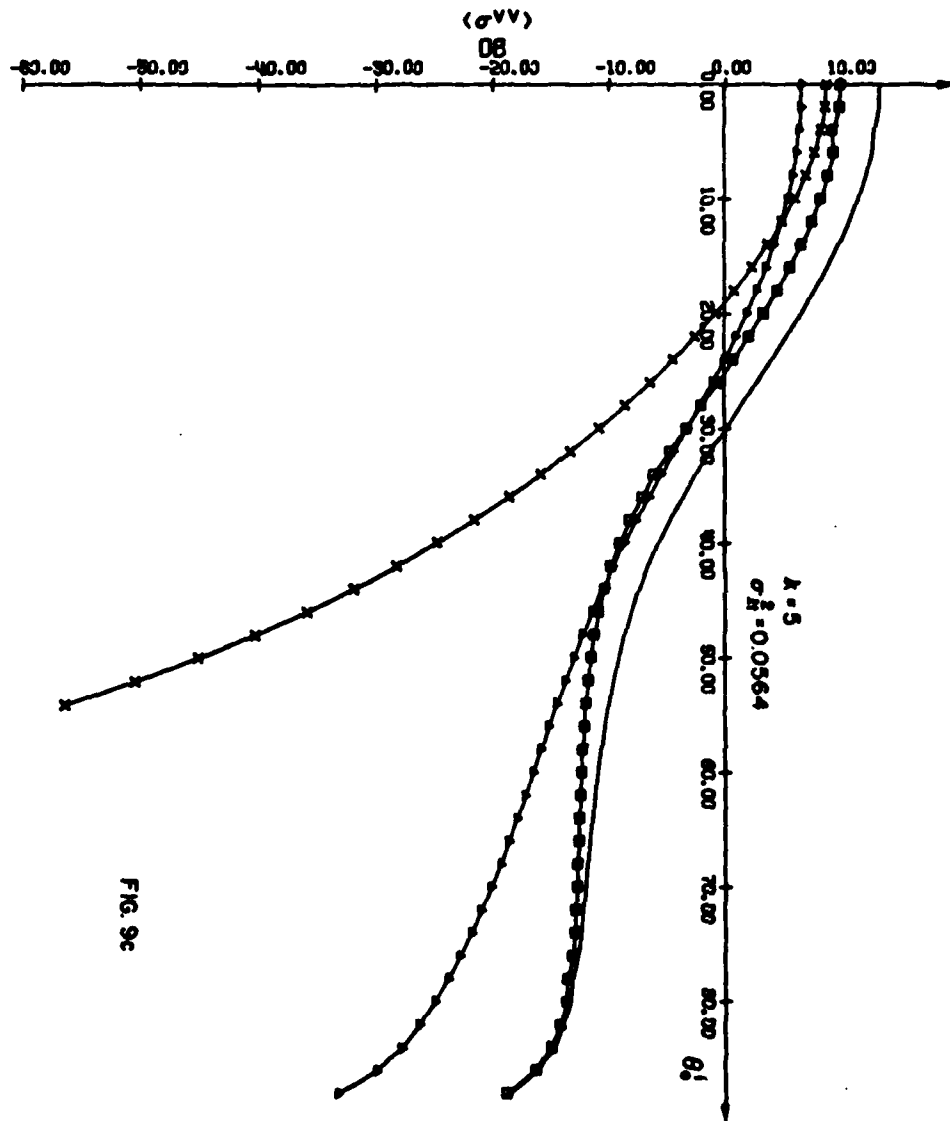


FIG. 9c

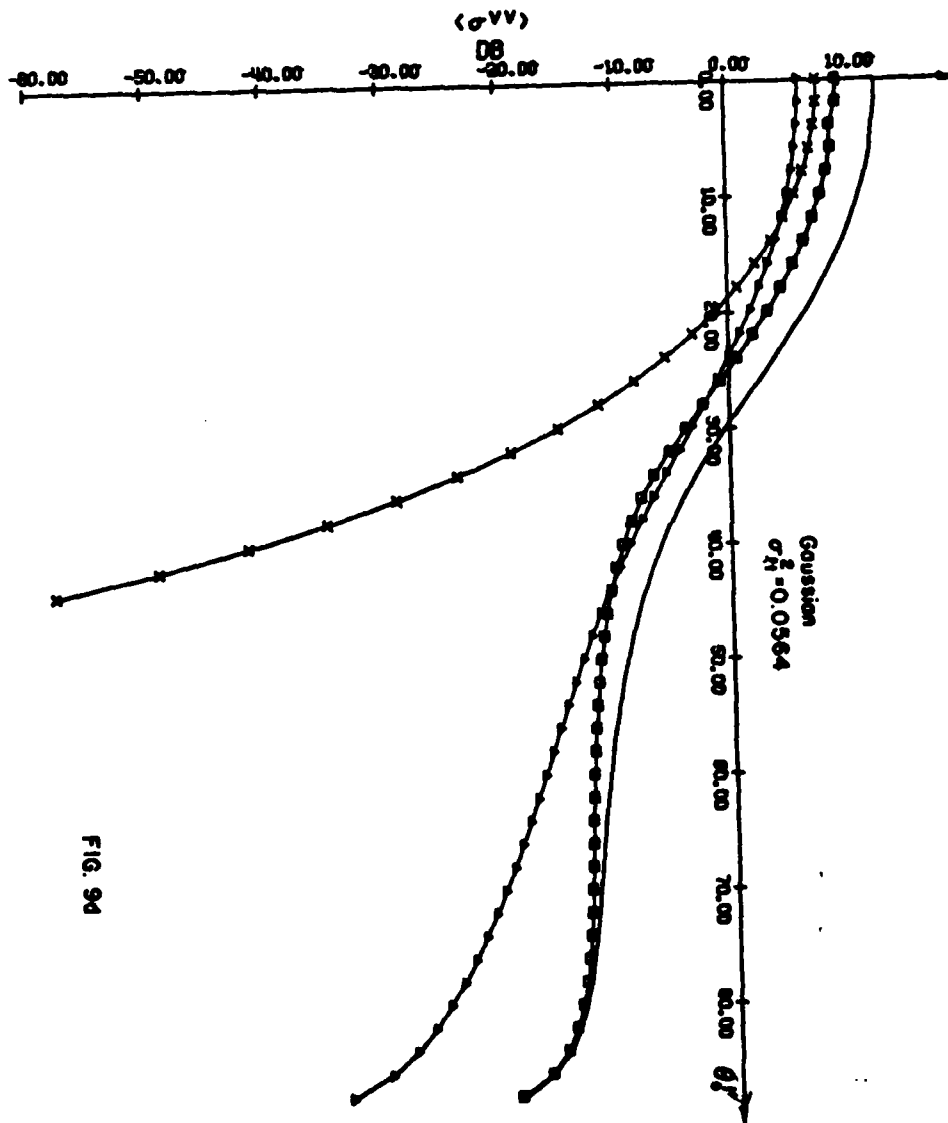
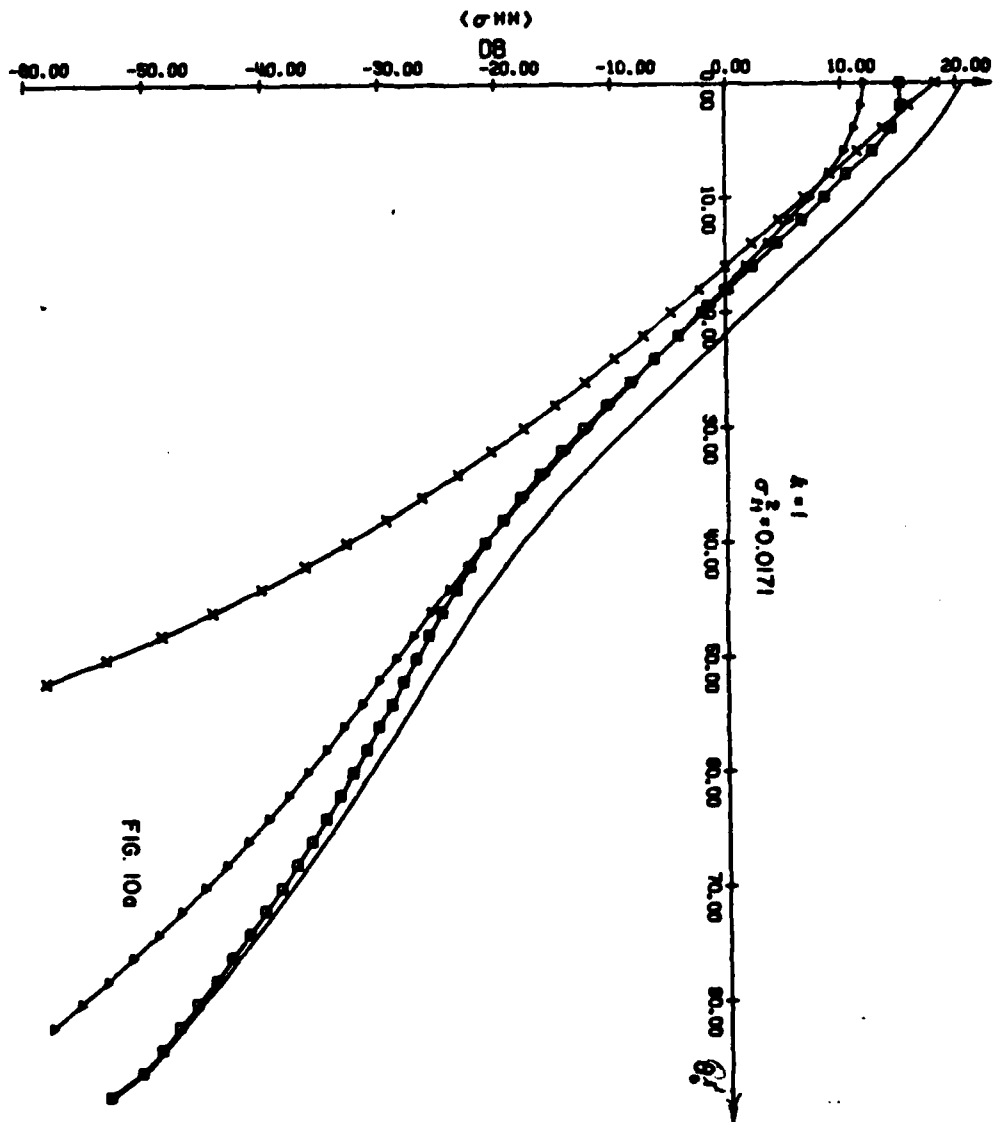
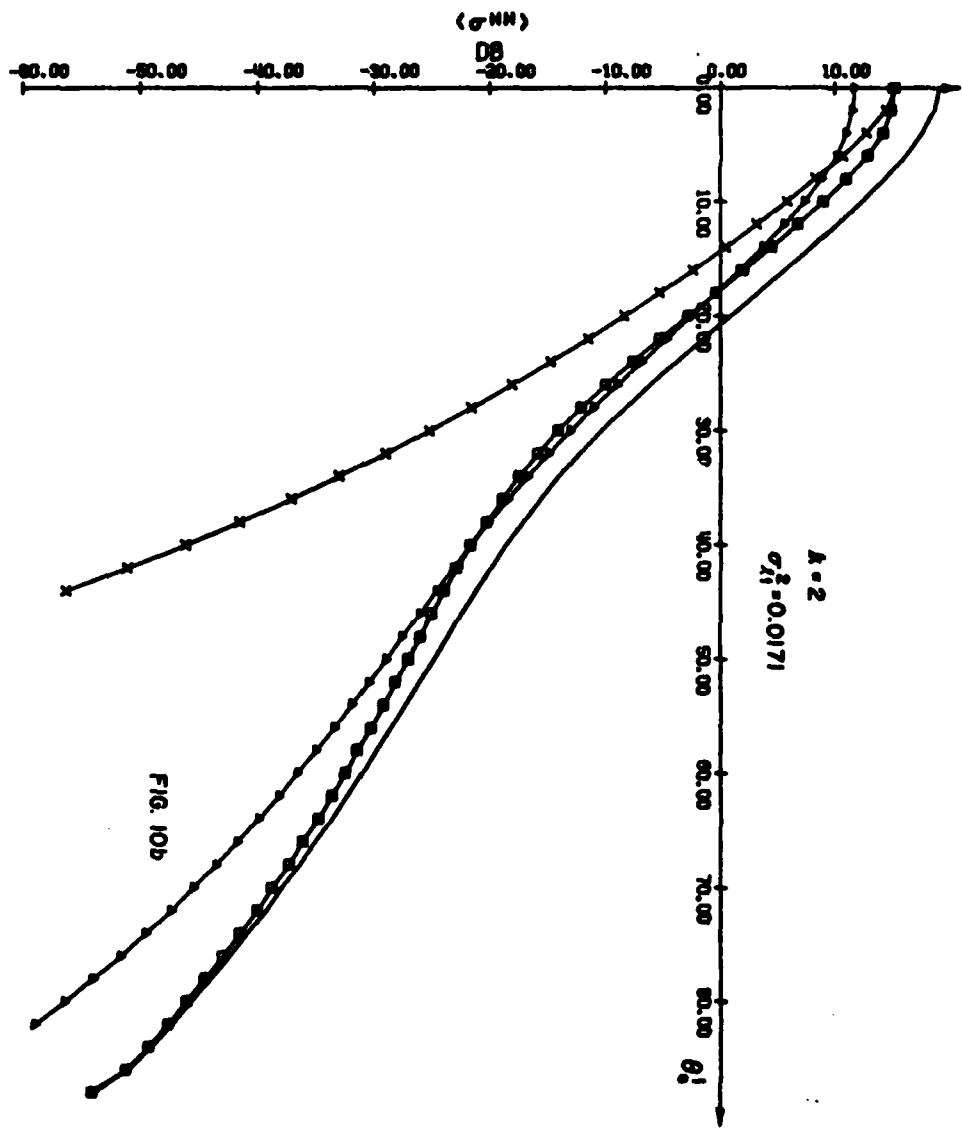


FIG. 94





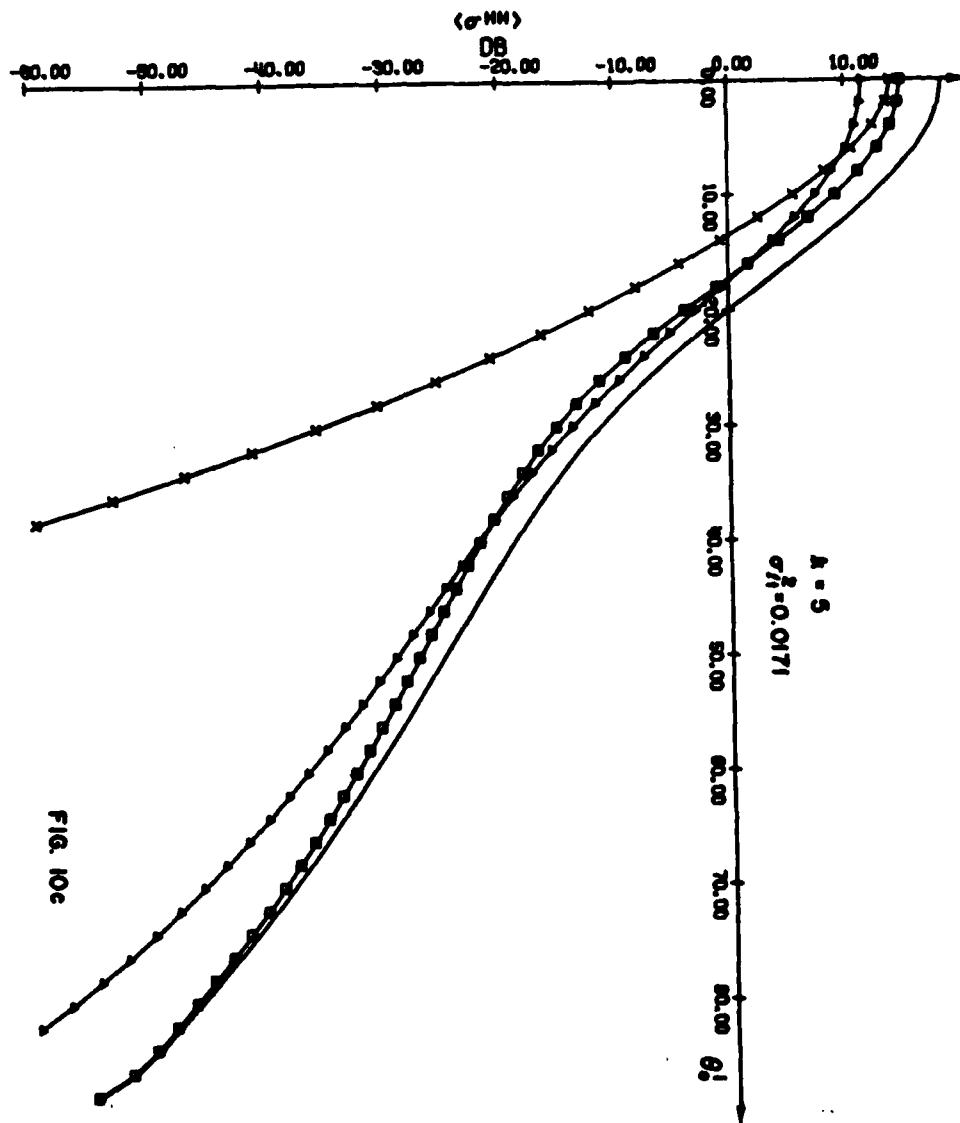


FIG. 10c

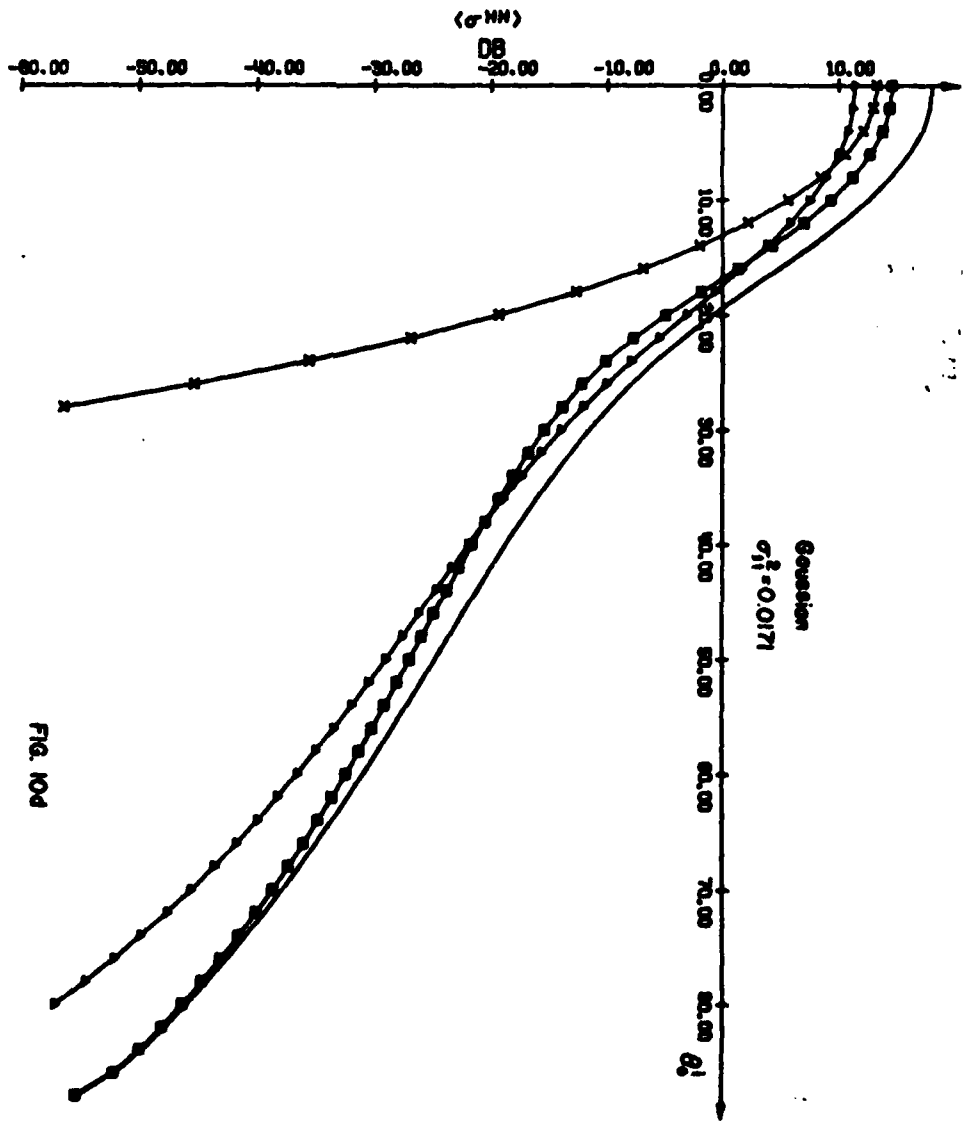


FIG. 104

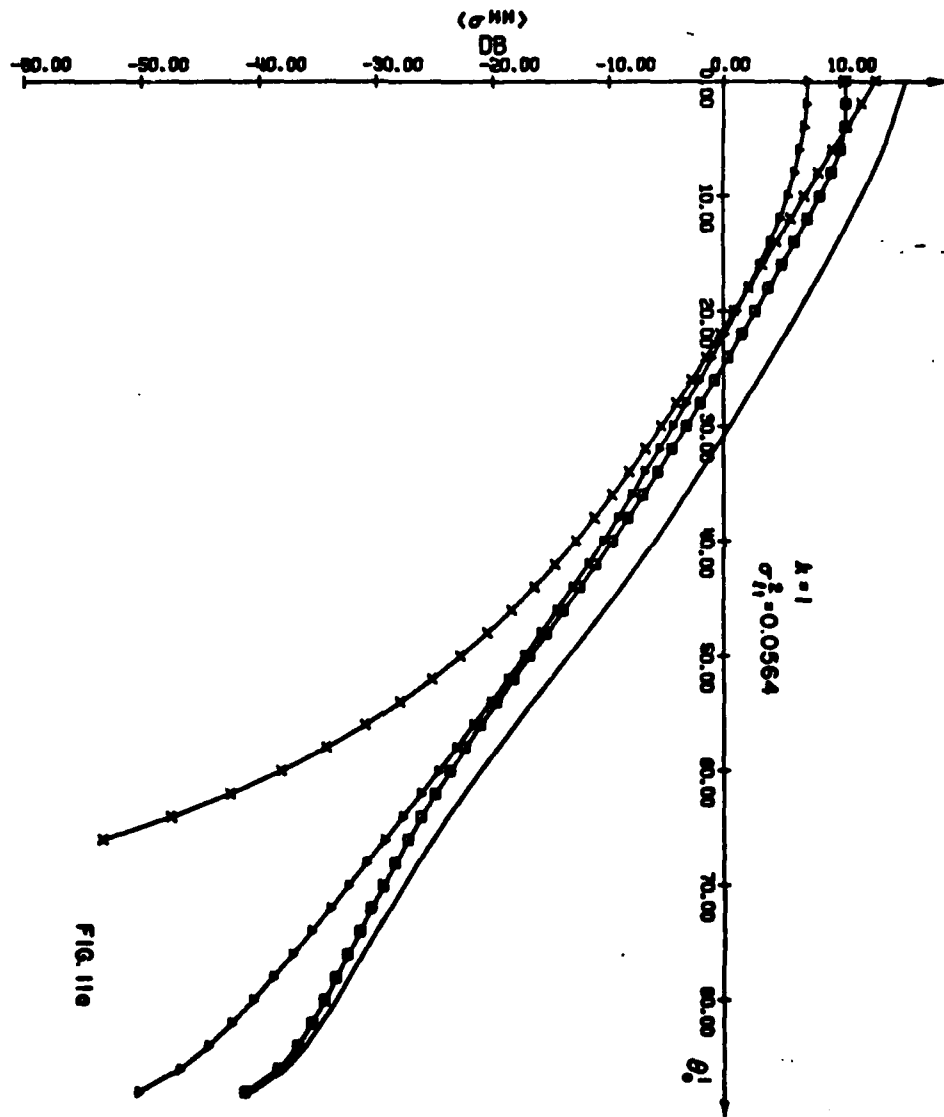


FIG. 11e

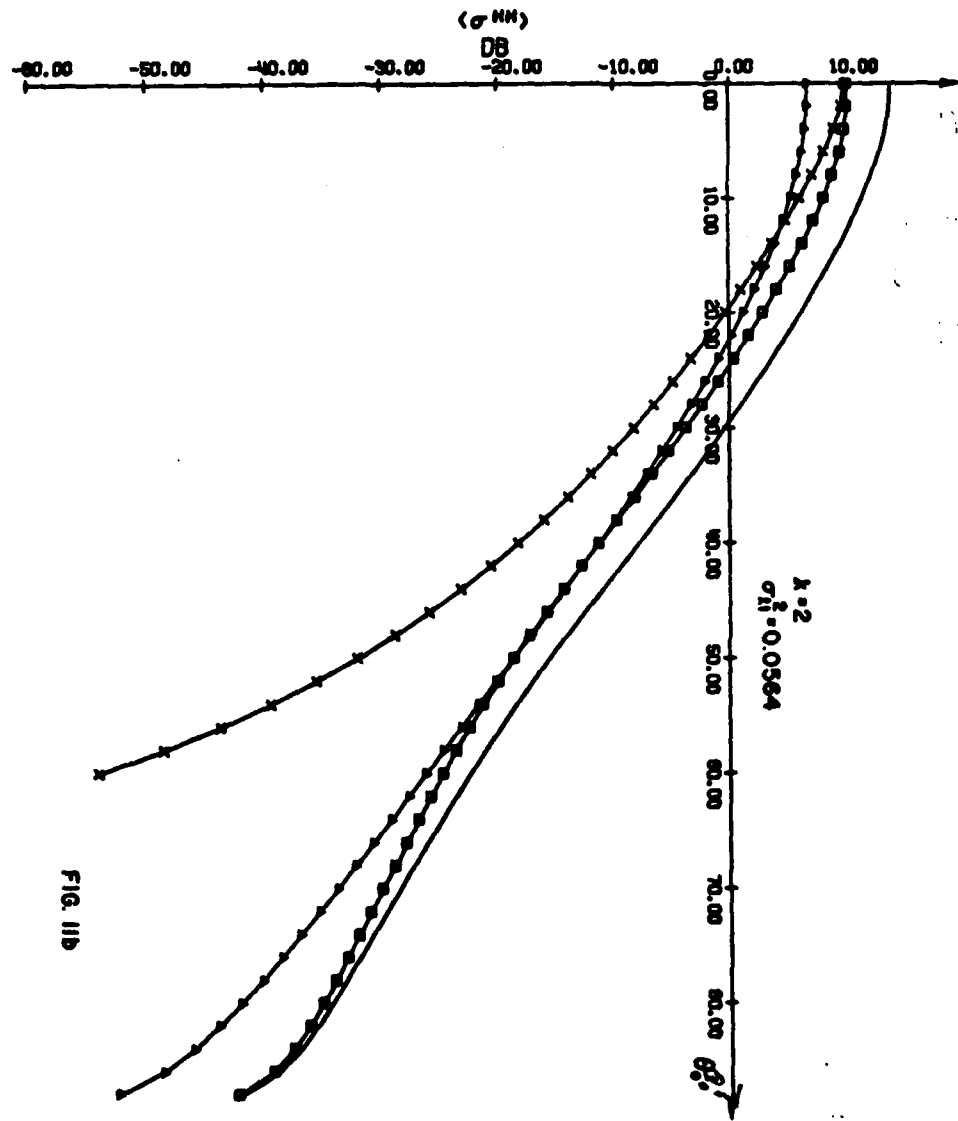
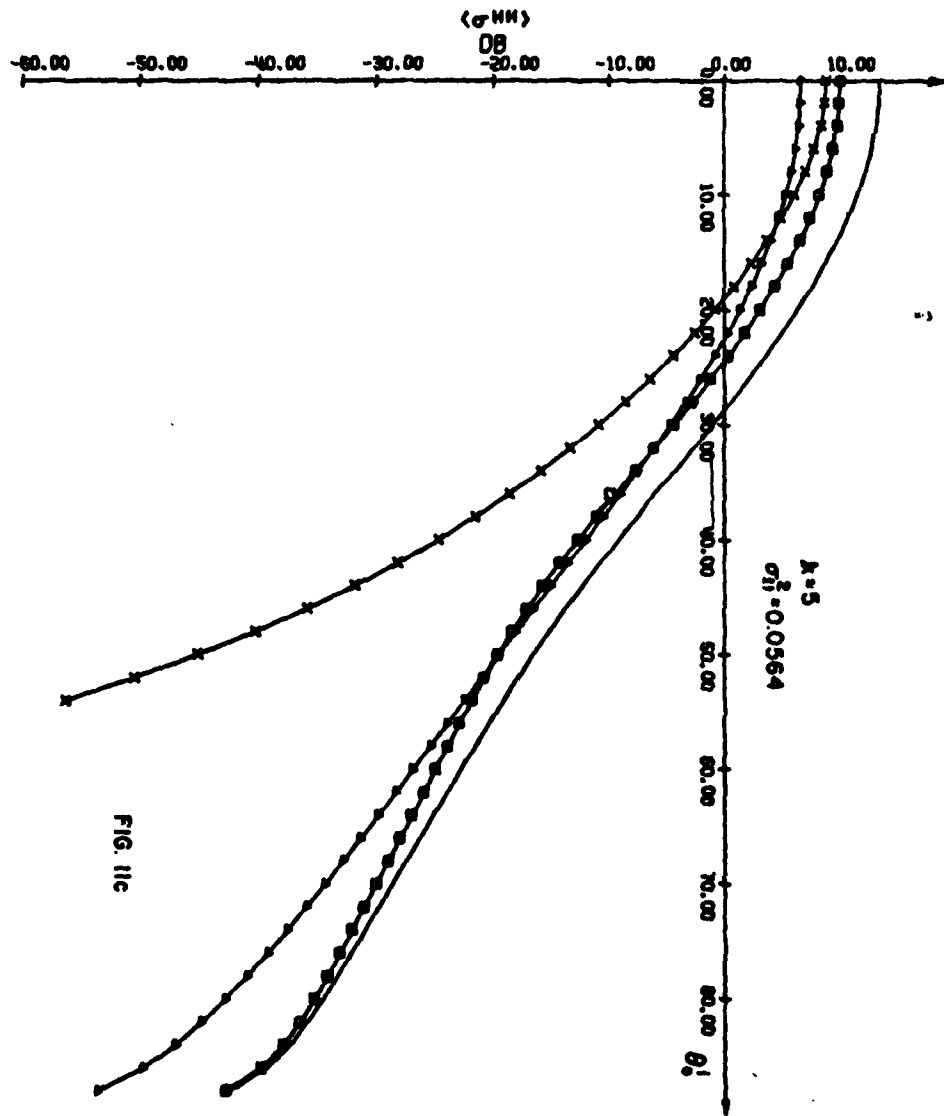


FIG. 11b



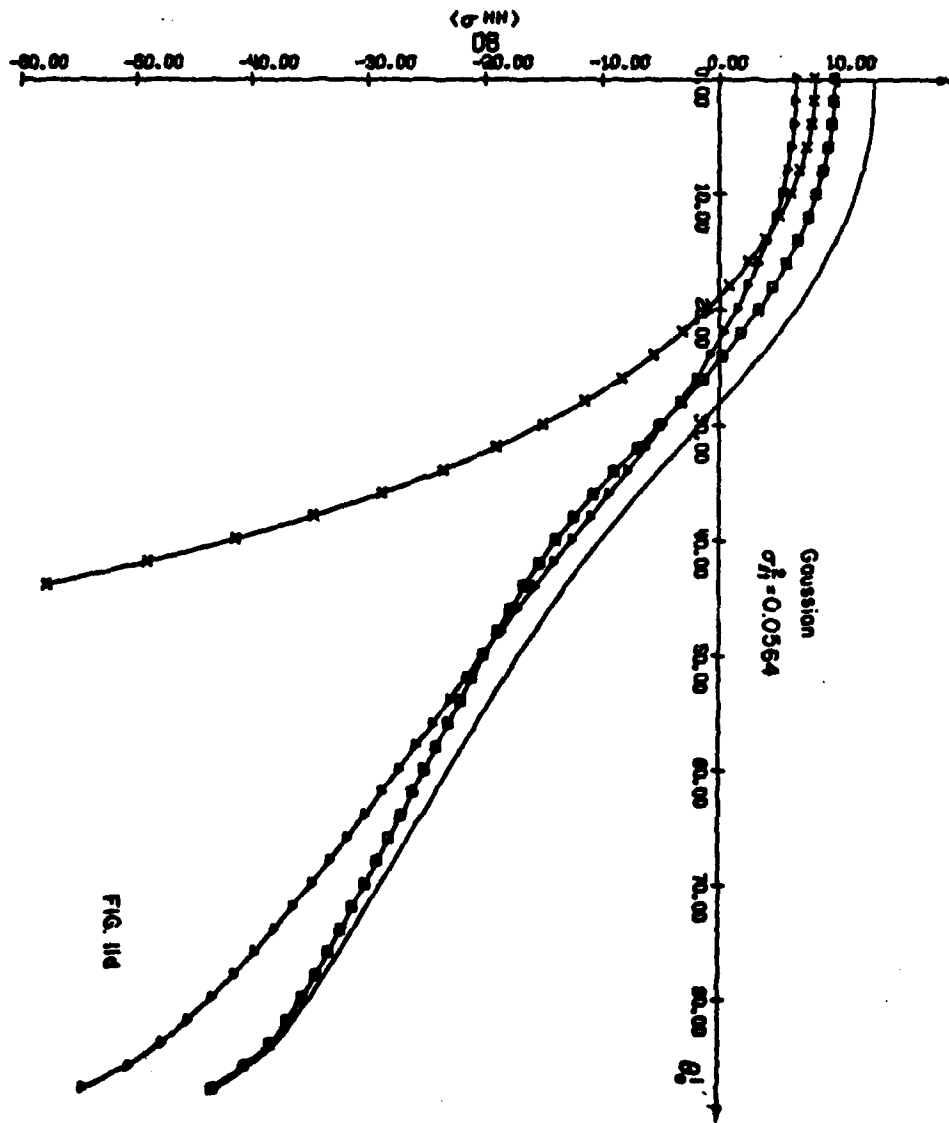


FIG. 11d

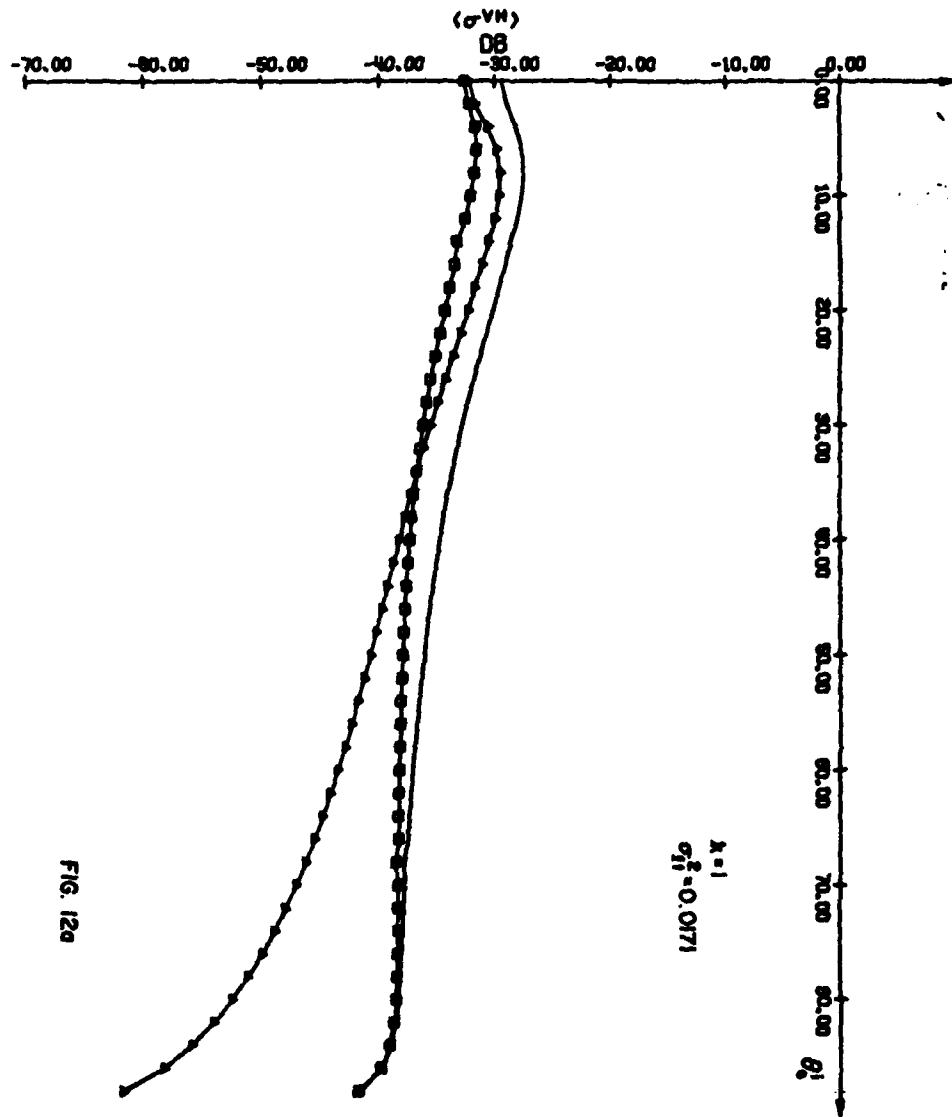


FIG. 12a

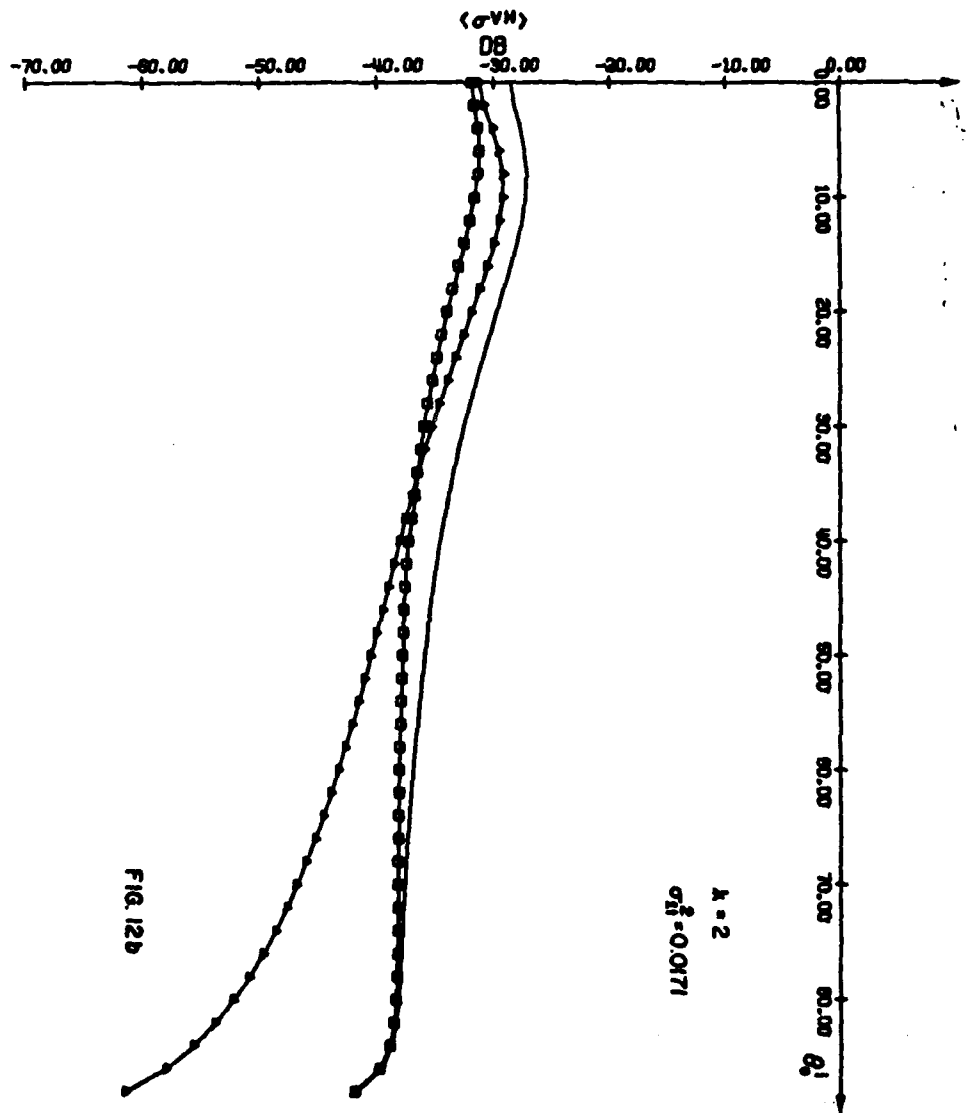


FIG. 12b

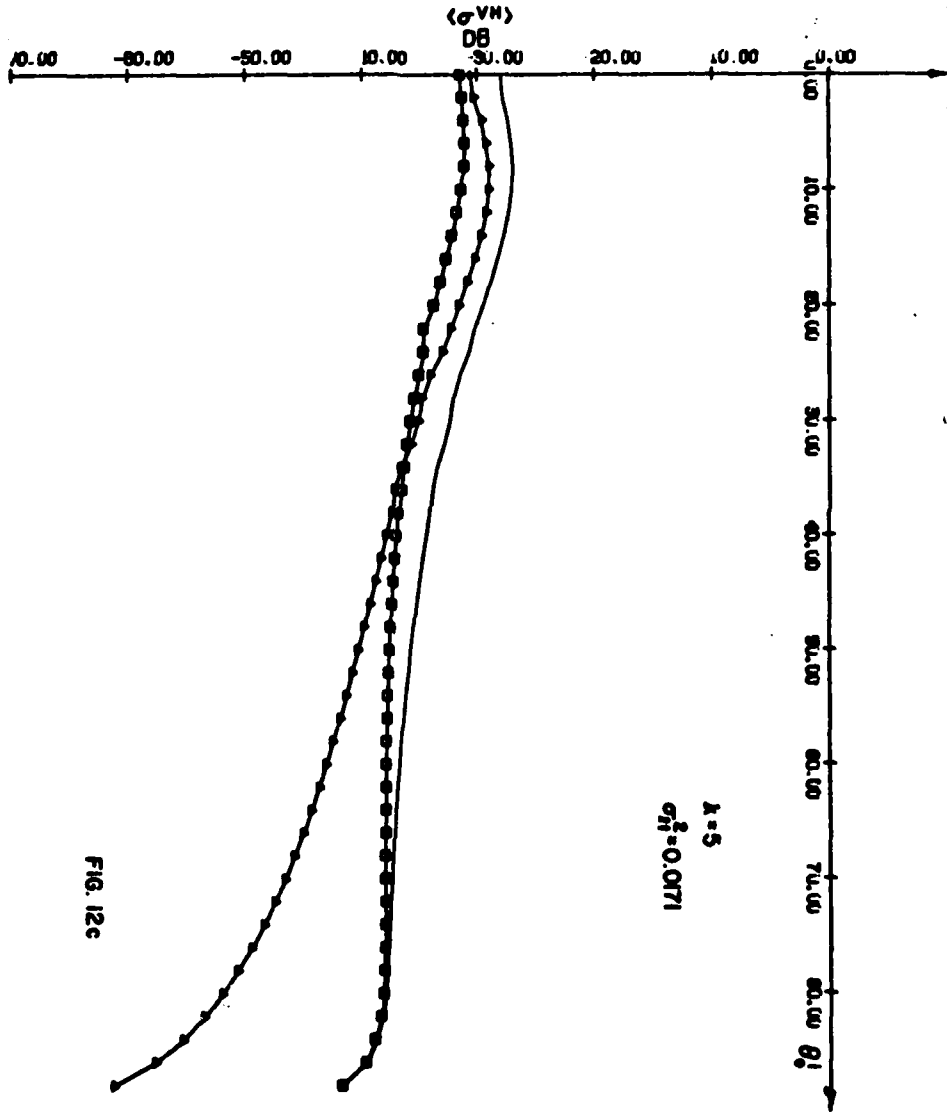


FIG. 12c

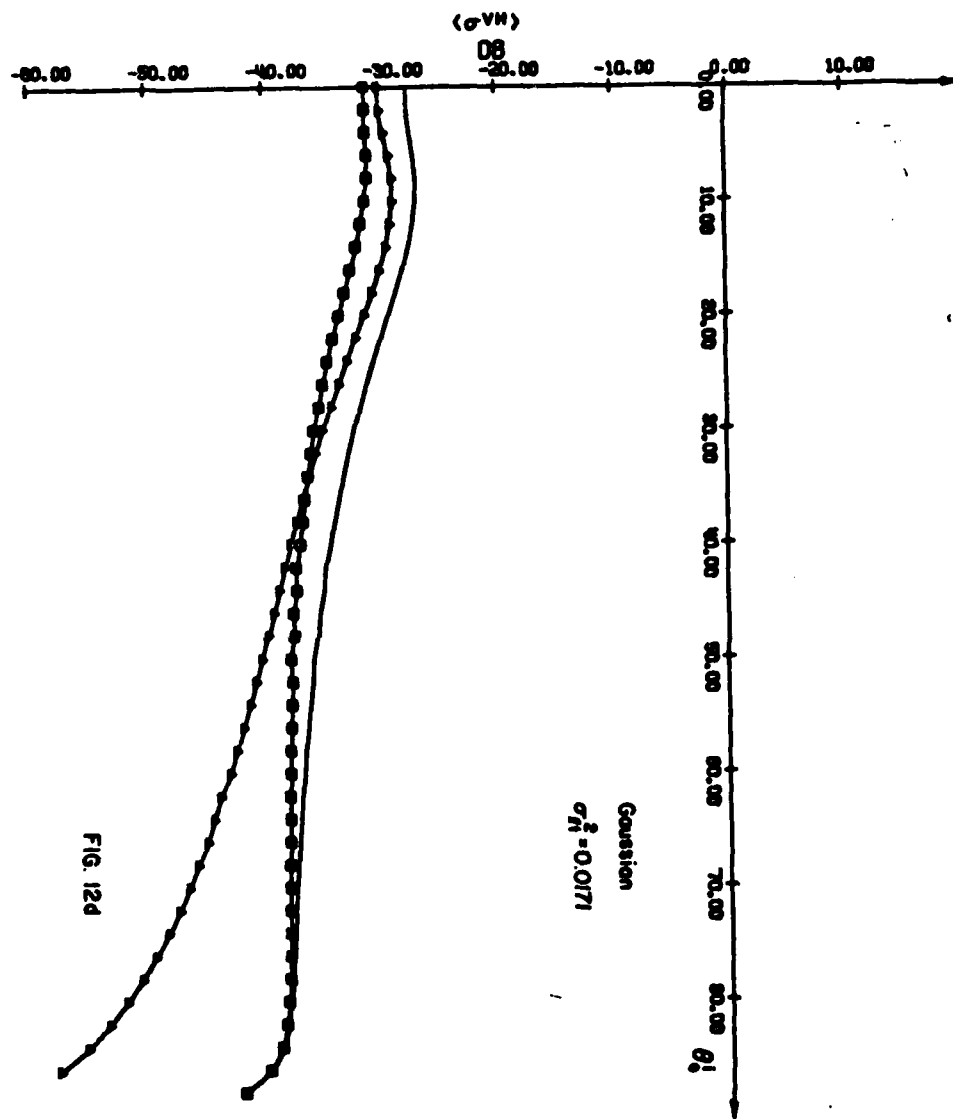


FIG. 124

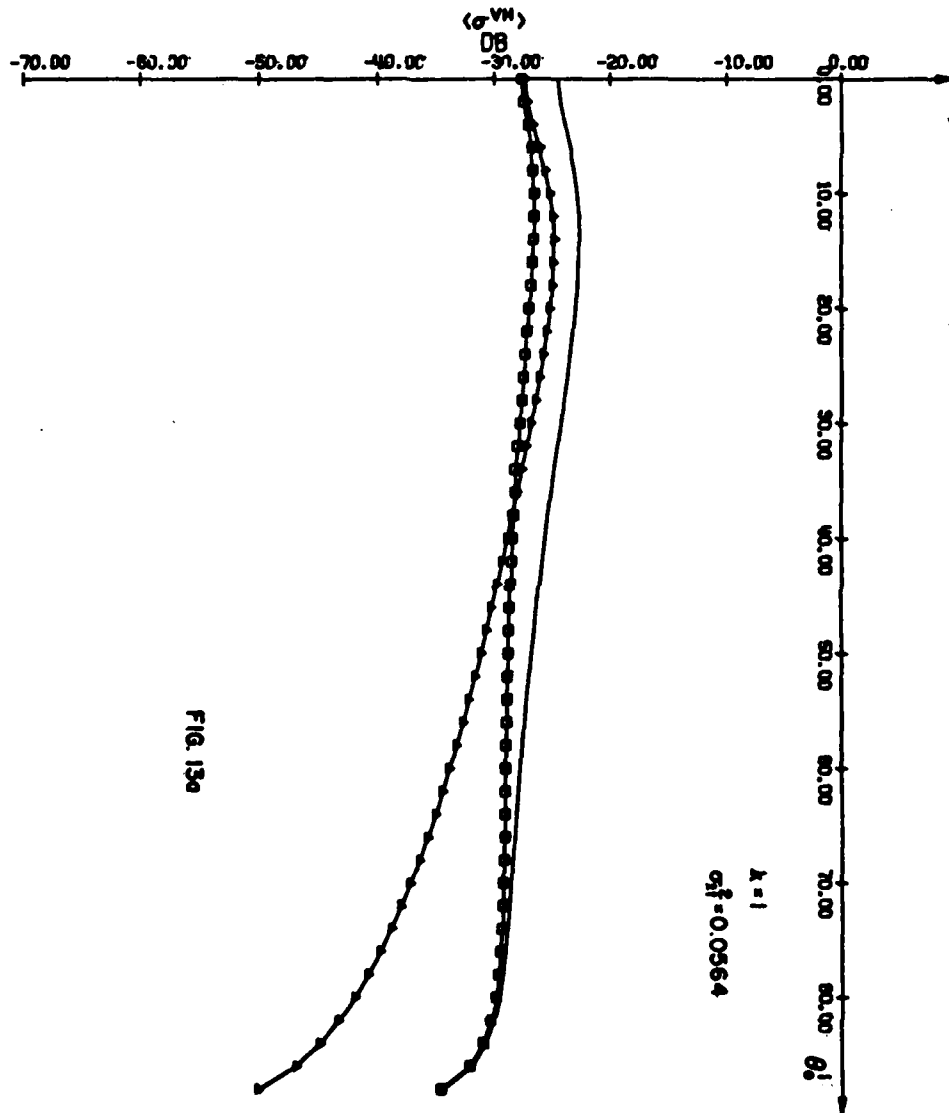


FIG. 13a

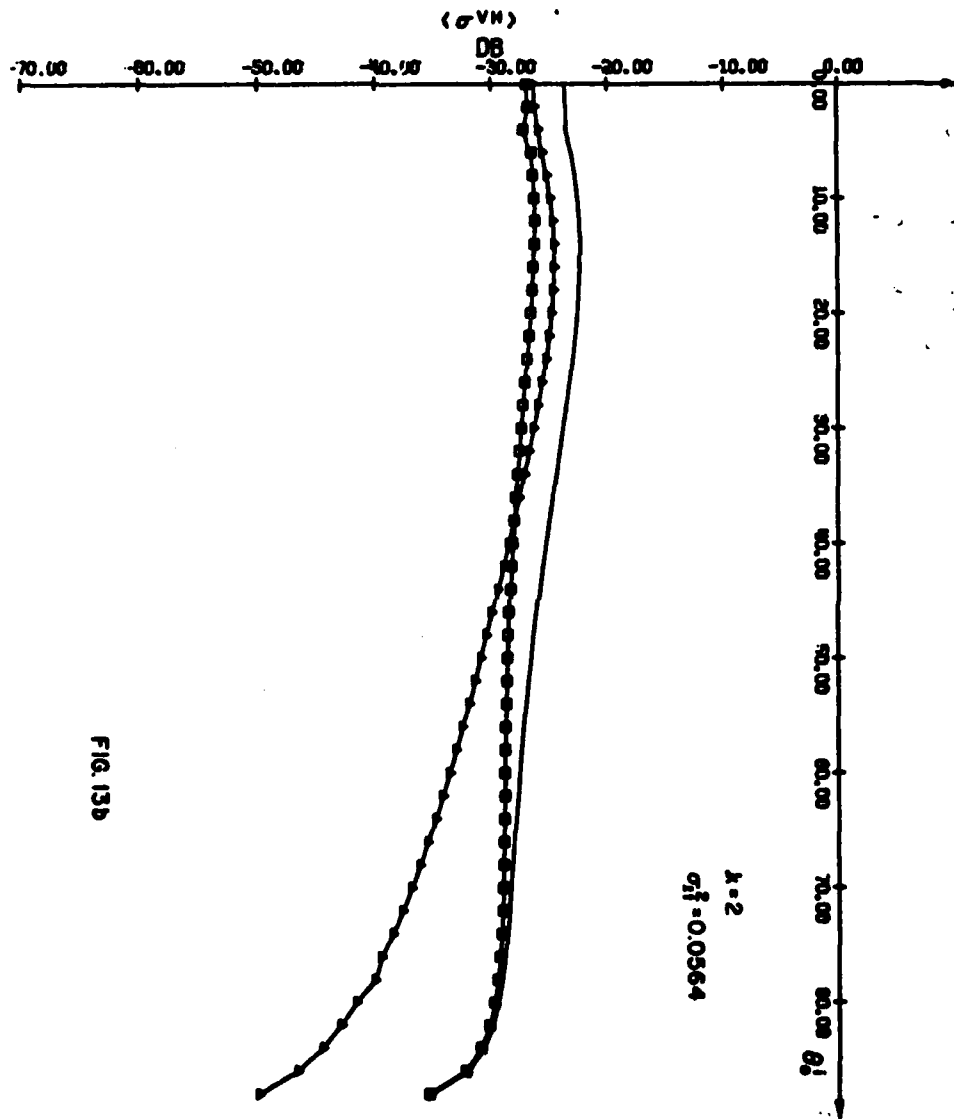


FIG. 13b

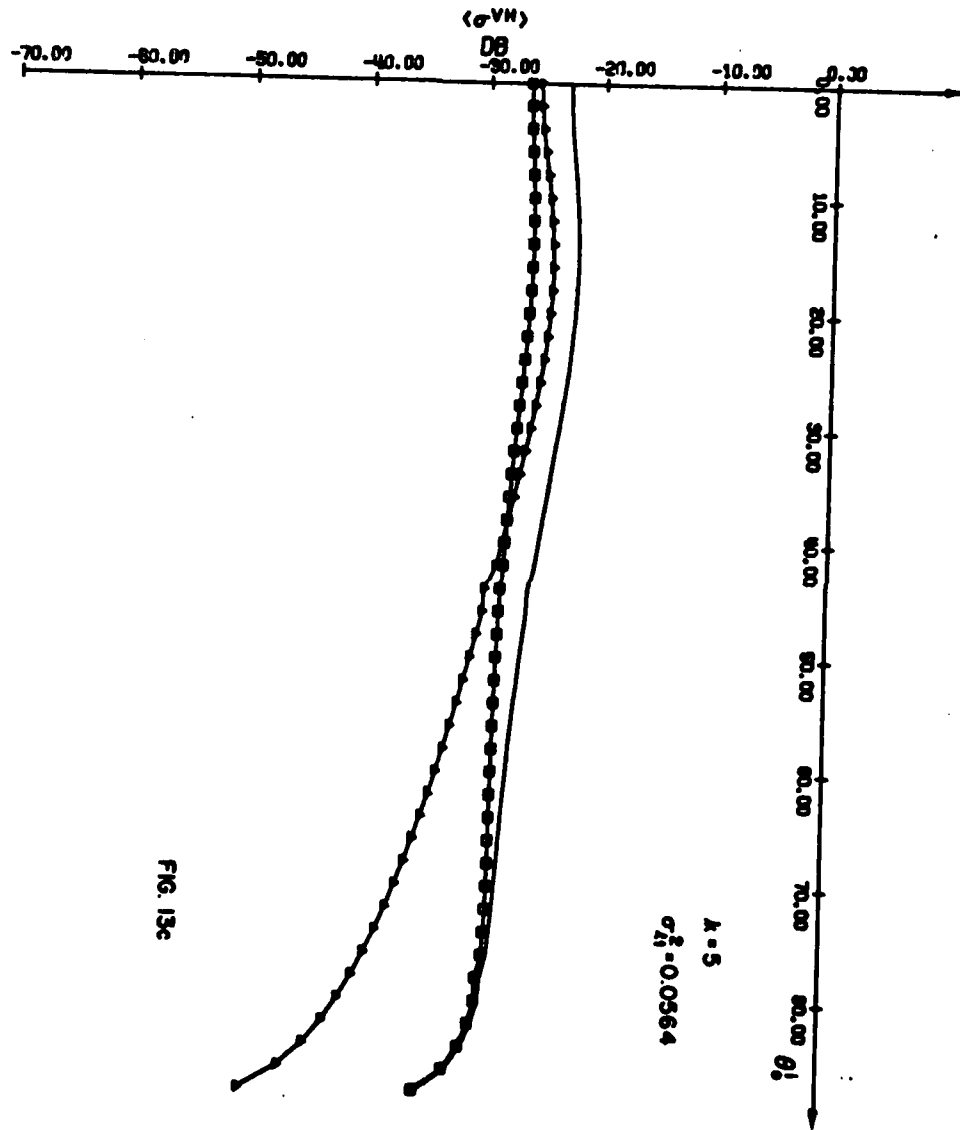


FIG. 13c

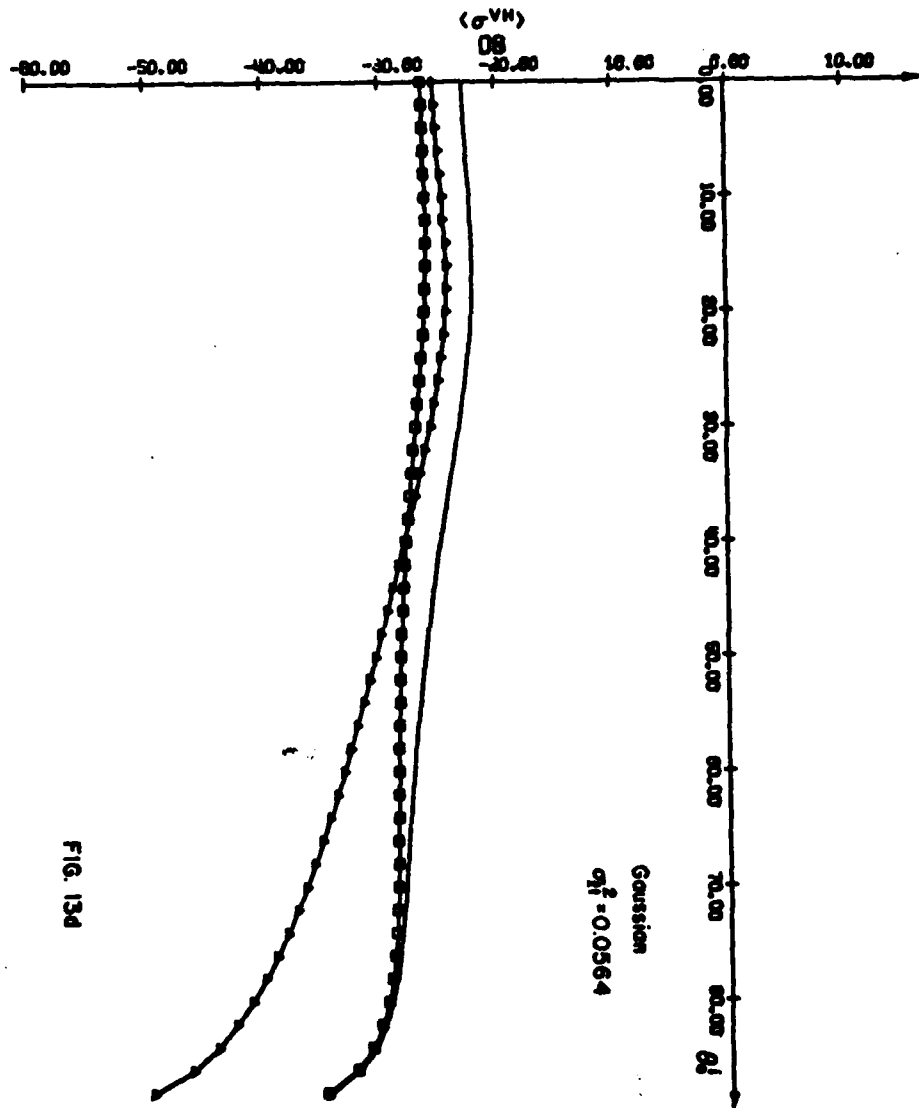


FIG. 134

